Research Square

Preprints are preliminary reports that have not undergone peer review.
They should not be considered conclusive, used to inform clinical practice,
or referenced by the media as validated information.

Low-Carbon Kaolin Subgrade Stabilization Using Micro- and Nano-Stabilizers: Experimental, Numerical and Life Cycle Assessment

Abolfazl Soltani
Shahid Rajaee Teacher Training University
Arash Aminaee
Shahid Rajaee Teacher Training University
Atousa Alesoltan
Shahid Rajaee Teacher Training University
Nabioallah Ahmadi
Shahid Rajaee Teacher Training University
Chinchu Cherian
chinchu.cherian@unbc.ca
University of Northern British Columbia

Research Article

Keywords: Life Cycle Assessment, Sustainable Ground Improvement, Finite Element Modeling, Nano Tuff, Nano Kaolin, Micro Silica, Resource Management

Posted Date: May 11th, 2026

DOI: https://doi.org/10.21203/rs.3.rs-9363555/v1

License: This work is licensed under a Creative Commons Attribution 4.0 International License.
Read Full License

Additional Declarations: No competing interests reported.

Low-Carbon Kaolin Subgrade Stabilization Using Micro- and Nano-Stabilizers: Experimental, Numerical and Life Cycle Assessment

Abolfazl Soltani[a], Arash Aminaee[b], Atousa Alesoltan[c], Nabioallah Ahmadi[d], Chinchu Cherian[e*]

[a,b,c,d] Faculty of Civil Engineering, Shahid Rajaee Teacher Training University (SRTTU), 1678815811, Tehran, Iran

[e] School of Engineering, University of Northern British Columbia (UNBC), Prince George, BC, Canada

[a]asoltani@sru.ac.ir, [b]arash.aminaee@gmail.com, [c]asa.alsoltan@gmail.com, [d]nahmadi@sru.ac.ir,
[e]chinchu.cherian@unbc.ca ([*]Corresponding author), 16-digit ORCID Id: 0000-0001-8617-0374

ABSTRACT

This study investigates the use of nano kaolin (NK) and nano tuff (NT) as low-carbon natural pozzolans for stabilizing weak kaolin subgrades, with the objective of partially or fully replacing conventional binders, hydrated lime (L) and micro silica (MS). Various mix designs were defined based on additive dosage (by dry soil mass) and evaluated over multiple curing periods. A multi-scale assessment framework was adopted, integrating laboratory testing, finite element modeling, and cradle-to-site life cycle assessment (LCA) to quantify mechanical performance, deformation behavior, and environmental impact.

Experimental results show that nano-based mixtures enhance subgrade performance, particularly in lime-activated systems. Lime-treated mixes exhibited significant reductions in plasticity. The binary mixture of 7% MS and 3% L achieved the highest unconfined compressive strength (2.7 MPa), representing a 6.3-fold increase over untreated soil, and a soaked CBR of 42% after 28 days (14-fold improvement). Microstructural analysis confirmed the formation of C-A-S-H and N-A-S-H gels due to the pozzolanic reactivity of MS, NK, and NT. Finite element simulations indicated that this optimal mix reduced subgrade vertical strain by over 90%, enabling a decrease in base layer thickness from 647 mm to 196 mm. However, LCA results reveal an engineering–sustainability trade-off: while lime-based systems provided superior mechanical performance, they resulted in higher environmental impacts, particularly in global warming potential (GWP). In contrast, lime-free single-stabilizer systems (3% NK and 3% NT) achieved up to 88% lower GWP, offering a more sustainable alternative. Overall, NK and NT demonstrate strong potential as low-carbon stabilizers, balancing performance improvement with reduced environmental impact.

Keywords: Life Cycle Assessment, Sustainable Ground Improvement, Finite Element Modeling, Nano Tuff, Nano Kaolin, Micro Silica, Resource Management.

1. Introduction

Poor mechanical properties of subgrade soils can weaken the engineering performance of pavement systems, reduce road serviceability and lifespan, and lead to high annual renovation costs [1,2]. Consequently, engineers continue seeking innovative methods to stabilize weak subgrades and one commonly recognized stabilization method is chemical stabilization.

Several studies have shown that the weak mechanical properties of soils can be effectively improved by using various geomaterials, such as hydrated lime and pozzolans [3,4]. Hydrated lime is an alkaline geomaterial widely used in subgrade stabilization practices for many years. Although it shows great capacity to enhance the soil strength, its CO_2 emissions and adverse impacts on vegetation conflict with environmental and sustainability goals. To address these limitations, researchers have explored partial or full replacement of lime with alternative pozzolanic materials to enhance subgrade performance while reducing environmental impacts [3,5]. This study aims to investigate the effects of some selected natural and industrial pozzolans, with or without hydrated lime, on improving the weak engineering behavior of kaolin subgrade soils.

Many researchers have shown that kaolin soil is soft and collapsible, making it unsuitable for subgrade [6–8]. Industrial pozzolans (e.g., micro silica (MS)) or natural pozzolans (e.g., nano shale or sepiolite fibres) have been reported to effectively improve the mechanical properties of kaolin soil, with or without hydrated lime [3,9,10]. For example, Zaini et al. [11] reported that the unconfined compressive strength (UCS) of the kaolin soil mixed with 6 wt% MS and 9 wt% quicklime was developed more than 4 times after 30 days of curing, compared to untreated kaolin soil. They further noted that mixing 6 wt% MS alone with kaolin soil improved UCS by about 86% after 30 days. Although MS, a by-product of ferrosilicon and ferroalloy production, has proven effective in soil improvement practices, its limited availability in some regions restricts its widespread application. Instead, natural pozzolans, widely available and often more sustainable, can provide more practical solutions for subgrade stabilization. Among these, nano kaolin (NK) and nano tuff (NT) are the focus of this study.

Kaolinite [$Al_2Si_2O_5(OH)_4$] is an aluminosilicate-rich mineral characterized by its laminar layers and dispersed arrangement [8]. Several studies have investigated calcined kaolinite (metakaolin) for stabilizing weak soils. For example, Jangde and Khan [12] found that the UCS increased by 78% with the addition of 15 wt% metakaolin to the clay soil. Similarly, Dao et al. [13] also reported that adding 6 wt% metakaolin to the lateritic soil increased the 28-day UCS and unsoaked California bearing ratio (CBR) values by 45% and 139%, respectively. Although calcined kaolinite demonstrates considerable potential for soil stabilization, its production requires substantial energy, as kaolinite must be heated at 650-850 $^{\circ}$C for several hours [14]. While metakaolin has been widely studied, its large carbon footprint and high processing cost limit its sustainability. Alternatively, this study aims to investigate the feasibility of using NK as an eco-friendly stabilizer in kaolin soil subgrade to mitigate the adverse impacts of calcined materials. Furthermore, the effects of NK in combination with hydrated lime are scarcely reported in the literature, highlighting an important knowledge gap addressed in this study.

Tuff is another aluminosilicate-rich material whose pozzolanic potential for subgrade improvement, with or without hydrated lime, is assessed in this study. Salimi et al. [15] noted that volcanic tuff contains abundant SiO_2, Al_2O_3, and Fe_2O_3 contents (> 76 wt%), suggesting good potential for pozzolanic reactions. They observed that adding 20 wt% tuff to clay doubled

the UCS after 28 days of curing, primarily due to C-S-H gel formation. Further, Rabab'ah et al. [16] showed that adding 4 wt% lime and 25 wt% zeolitic tuff to expansive soil increased UCS and CBR by 22% and 70%, respectively. While such findings highlight the potential of tuff, the effects of NT on kaolin soils, with or without hydrated lime, remain underexplored. This study, therefore, investigates NT as a natural pozzolan for subgrade stabilization and benchmarks its performance against traditional hydrated lime and industrial MS.

Accordingly, this study focuses on the experimental evaluation of NK, NT, and MS, in the presence or absence of hydrated lime, for kaolin subgrade stabilization. A comprehensive series of laboratory tests was performed, including Atterberg limits, compaction properties, UCS, modulus of elasticity, and CBR. In addition, the physicochemical characteristics of untreated soil, additives, and stabilized subgrade mixes were evaluated using pH tests, Brunauer-Emmett-Teller (BET) analysis, X-ray diffraction (XRD), and X-ray fluorescence (XRF) analyses. Microstructural observations were also carried out using field emission scanning electron microscopy (FE-SEM) coupled with the energy dispersive X-ray (EDX) microanalysis.

To assess the practical performance of the stabilized subgrade, a simple numerical analysis using finite element Modeling (FEM) was performed in PLAXIS 2D, following the pavement design guidelines recommended by Austroads [17]. Moreover, the environmental impacts of applying these stabilizers in subgrade applications were evaluated using a cradle-to-site Life Cycle Assessment (LCA) via SimaPro 9 software. Although LCA has been increasingly applied in geotechnical and pavement studies [18], its integration with chemical stabilization of kaolin subgrades remains limited in the literature. Unlike conventional strength-based evaluations, LCA provides a broader perspective by quantifying the environmental burdens associated with producing and applying stabilizers, such as greenhouse gas emissions, energy consumption, and resource depletion. Given that hydrated lime, while mechanically effective, is linked to high CO_2 emissions, it is crucial to benchmark its environmental impact against alternative pozzolanic materials.

The outcomes of this study will contribute to a better understanding of the feasibility and environmental implications of MS, NK and NT as alternative stabilizers in pavement construction. By reusing waste industrial materials, conserving natural resources, and exploring locally available geomaterials, this research aims to provide more sustainable alternatives to replace conventional hydrated lime while maintaining or improving subgrade performance.

2. Materials and Methods

2.1. Materials

2.1.1. Kaolin Soil and Nano Kaolin

Kaolin soil was taken from the Mershon quarry, located in Zanjan Province, Iran. It is a residual soil, excavated from a depth of 1.5 to 2 meters below the ground level. The collected samples were sealed in plastic bags. A total of 15 soil samples (~150 kg) were taken, keeping the spatial distance of 10 meters. The soil samples were passed through a mesh No. 4 (4.76 mm sieve) to remove the agglomerations. The particle size distribution of the Mershon kaolin soil shows that the soil contains 6% fine sand, 8% silt, and 86% clay particles, determined according to the ASTM C136 [19] for analyses of coarse grains and the ASTM D7928 [20] for

hydrometric analyses. Figure 1 illustrates the major crystalline phases of Mershon kaolin soil. The XRD pattern (Fig. 1) shows that the selected soil mainly consists of microcrystalline minerals of quartz, kaolinite, and enstatite. Furthermore, the chemical compositions of the Mershon kaolin soil were presented in Table 1. Chemically, the most dominant oxides present in kaolin soil include SiO_2 (69.06 wt%), Al_2O_3 (20.89 wt%), and Fe_2O_3 (0.54 wt%). The total content of the three dominant oxides is 90.5 wt%, which indicates pozzolanic specification [21]. Table 2 represents the engineering characteristics of kaolin soil. According to the unified soil classification system [22], the Mershon kaolin soil is classified as clay with low plasticity (CL).

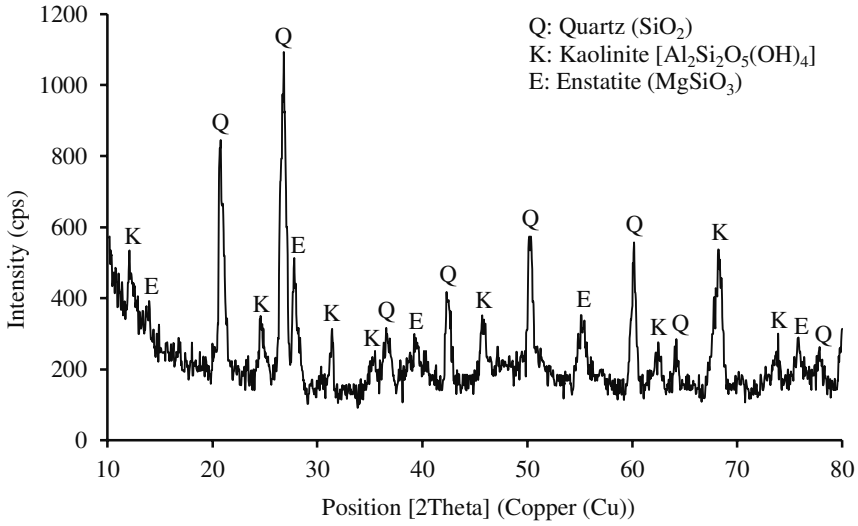


Fig. 1 XRD pattern for the pulverized Mershon kaolin soil

Table 1 XRF data for kaolin soil, tuff, micro silica and hydrated lime

Materials	Major oxides (wt%)										
	SiO_2	Al_2O_3	Fe_2O_3	CaO	Na_2O	K_2O	MgO	TiO_2	MnO	LOI	Total
Kaolin soil	69.06	20.89	0.54	0.98	1.29	1.47	1.20	0.10	0.02	3.97	99.52
Tuff	71.26	11.88	2.28	3.61	2.90	3.57	1.82	0.27	0.06	2.18	99.83
Micro silica	84.93	2.39	1.59	0.34	1.00	1.19	2.35	0.08	0.21	4.92	99.00
Hydrated lime	2.50	1.50	2.00	83.30	0.50	NA	0.50	na	na	9.40	99.70

Note: LOI = loss on ignition, na = not available

Table 2 Engineering properties of Mershon kaolin soil

Soil properties	Values	Standards
pH value	7.3	ASTM E70 [23]
Specific gravity (G_s)	2.74	ASTM D854 [24]
SSA (m^2/g)	6.58	ISO 9277:2022 [25]
Soil classification scheme (USCS)	CL	ASTM D2487 [22]
Sensitivity (S_t)	1.8-2.4	-
Liquid limit (LL%)	25.00	ASTM D4318 [26]
Plastic limit (PL%)	16.38	ASTM D4318 [26]
Plasticity index (PI%)	8.62	ASTM D4318 [26]
Maximum dry density (g/cm^3)	1.83	ASTM D698 [27]
Optimum moisture content (%)	15.89	ASTM D698 [27]
UCS (kPa)	440.69	ASTM D2166 [30]

Note: SSA = specific surface area

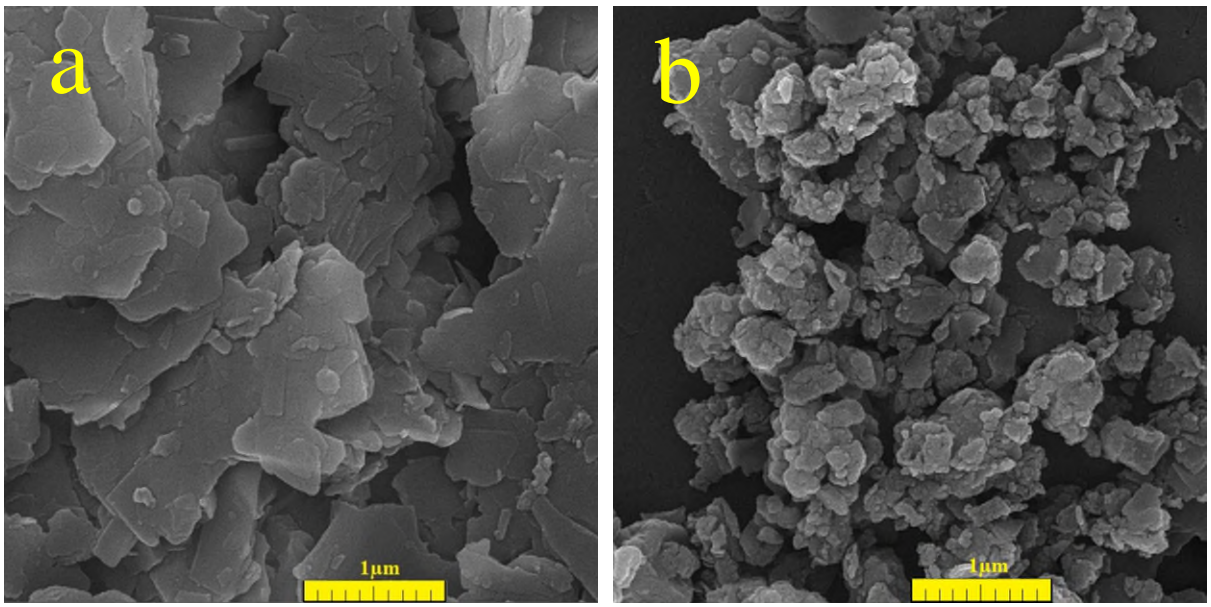


Fig. 2 FE-SEM images of a) Mershon kaolin soil and b) Nano kaolin

2.1.2. Nano Tuff

The volcanic green tuff samples (each of 15 kg) were extracted from the Karaj area, Alborz Mountain, Iran. The collected samples were mechanically ground in a rotary ball mill for about 5 hours at 33 rpm to obtain a fine, homogeneous powder. The powder was analyzed by dynamic light scattering (DLS), which indicated that the particle size of the tuff powder ranged from 1 to 100 nm (Table 3). The XRD pattern (Fig. 3) of nano tuff shows that major crystalline phases include quartz, kaolinite, enstatite, and wairakite (a zeolite mineral with an analcime structure but containing Ca^{2+}). According to Table 1, the XRF analysis indicates that the total content of SiO_2, Al_2O_3, and Fe_2O_3 in nano tuff was relatively high (85.42 wt%), and the LOI value was low (2.18 wt%), both characteristics of class C natural pozzolans [21]. Figure 4 exhibited the FE-SEM image for tuff powder after grinding. It is evident from Figure 4 that the textural feature of the tuff changed from agglomeration to a dispersed state with nano-sized particle diameters.

Table 3 Engineering properties of tuff, nano tuff, nano kaolin, micro silica, and hydrated lime

Materials	Bulk density (g/cm^3)	Specific gravity (G_s)	Specific surface area (m^2/g)	Mean effective diameter (nm)	pH
Tuff	2.4	2.4	na	na	9.5
Nano tuff	0.6	2.5	15.76	27.7	9.5
Nano kaolin	0.5	2.6	16.57	16.2	7.3
Micro silica	0.3	2.2	20.00	210.5	8.0
Hydrated lime	0.6	2.4	5.60	3650.3	12.4

Note: na = not available

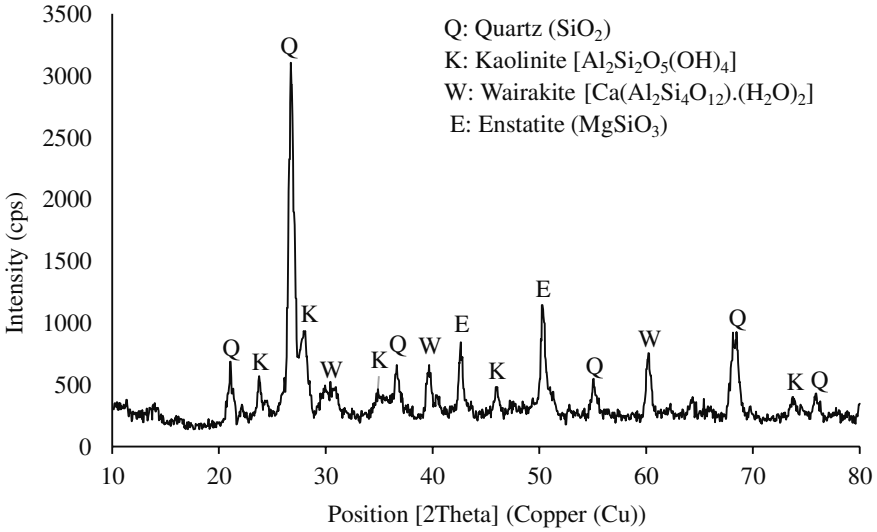


Fig. 3 XRD pattern for nano tuff

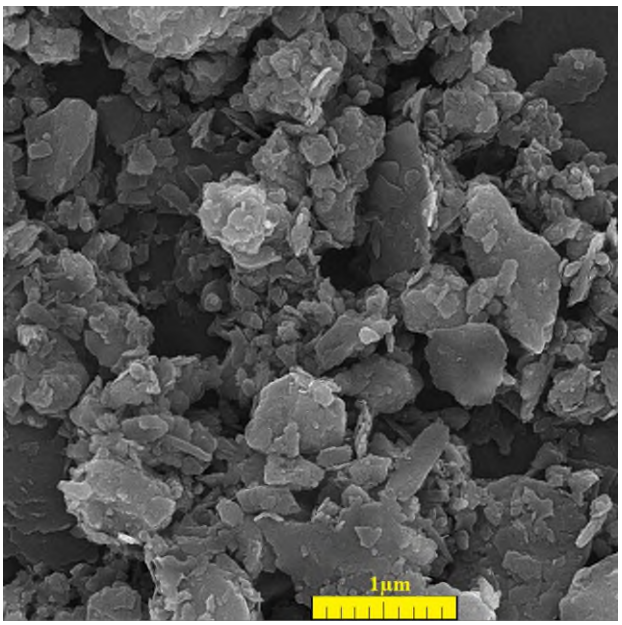


Fig. 4 FE-SEM image of nano tuff

2.1.3. Micro Silica

Micro silica (MS) was purchased from Iran Ferroalloy Industries Company, Azna, Iran. Table 1 presents the major oxides of MS, indicating that the total content of SiO_2, Al_2O_3, and Fe_2O_3 is high (88.91 wt%), suggesting a high pozzolanic potential [21]. Figure 5 illustrates the XRD pattern of MS, which shows a wide 2-Theta position (15-35 degrees), indicating that an amorphous phase is dominant. Table 3 shows the physical properties of MS, indicating a high specific surface area (SSA = 20 m^2/g) and a low bulk density (0.3 g/cm^3). In addition, Figure 6 displays the FE-SEM image of MS powder. It can be seen that the MS consists primarily of irregular spherical particles with varying diameters.

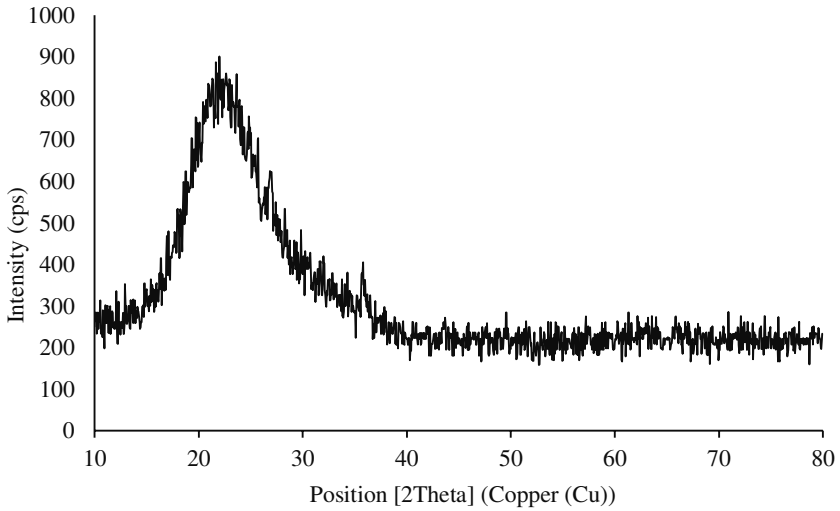


Fig. 5 XRD pattern for micro silica

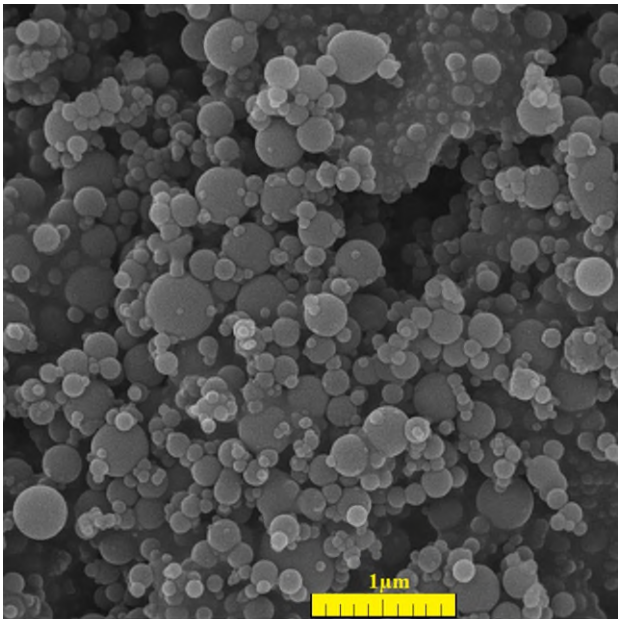


Fig. 6 FE-SEM image of micro silica

2.1.4. Hydrated Lime

The commercial hydrated lime [$Ca(OH)_2$] was purchased from a local lime factory, Qom, Iran. The chemical compositions and physical properties of selected hydrated lime were presented in Tables 1 and 3, respectively. Accordingly, the total alkaline oxides in hydrated lime, including CaO, MgO, and Na_2O, are high (84.3 wt%), resulting in a high pH (12.4). The high degree of alkalinity provides a suitable environment for potential pozzolanic reactions in clay-treated mixtures. The hydrated lime was completely passed through a sieve No. 200 (75 µm) to obtain a uniform and fine-grained powder.

2.2. Methods

Figure 7 presents a summary of the experimental, analytical, and computational methods employed in this study, illustrated through a simple flowchart.

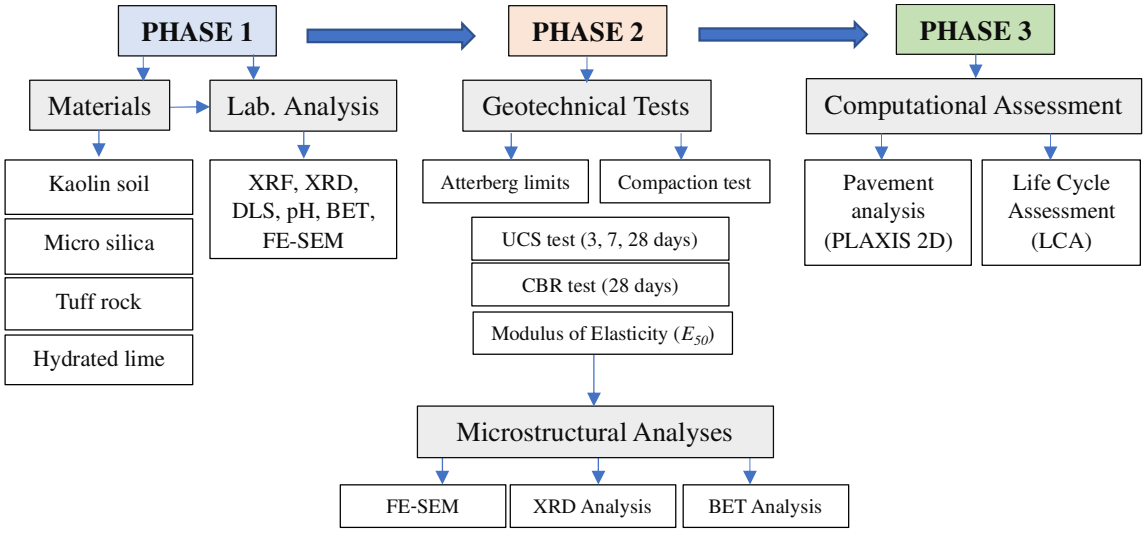


Fig. 7 Simple flowchart showing three major phases of the present study

2.2.1. Physiochemical Analyses

The major oxides of selected materials were determined by XRF analysis in accordance with ASTM E1621 [28]. The instrument used for XRF analysis was a Philips PW1410. In addition, the mineralogical properties of kaolin soil, NT, NK, MS, hydrated lime, and the final crystalline phases of the treated samples were detected by a Philips PW1730 diffractometer. Cu-Kα radiation (λ = 1.54 Å) was used for an angle scan (2θ) from 10° to 80°, with a step size of 0.05° and a 1 s per step time, for XRD analysis. The input voltage and the current were 40 kV and 30 mA, respectively. Furthermore, a TESCAN MIRA III machine coupled with an EDX analyzer was used to take FE-SEM images of the textures of primary materials and final products, as well as to detect the major and minor elemental compositions on the textural surfaces. The nanoscale to microscale images were taken of representative samples that were air-dried and coated with a thin gold layer. The process was conducted at an accelerating voltage of 20 kV and a working distance of 10 mm. At least four different points of each selected sample were analyzed to obtain more reliable results. Then, the average percentage of each heterogeneous sample was reported in the EDX analysis. The EDX results are reported as semi-quantitative values with an estimated detection limit of ~0.5 wt% for major elements. Moreover, the mean effective particle diameter of NT, NK, MS, and hydrated lime was determined by DLS in accordance with ISO 22412 [29]. The instrument used was MALVERN ZEN3600. Furthermore, a BET analyzer (BELSORP MINI II model) was employed to determine the SSA of micro and nano particles, along with pore size distribution. This analytical method is based on nitrogen gas adsorbed in the pores on the particle surface [25]. Moreover, the pH of kaolin soil, NT, NK, MS, hydrated lime, and treated samples was measured using a HI-8014 pH meter (Hanna Instruments) in accordance with ASTM E70 [23]. Measurements were performed on a 1:2.5 soil-to-deionized water suspension (10 g soil + 25 g deionized water), shaken for 30 min, and allowed to equilibrate for 30 min before testing. The instrument was calibrated daily with standard buffers (pH 4.01, 7.00, and 10.01). All tests were conducted at 25 ± 1 °C temperature with automatic temperature compensation, and each result represents the average of triplicate measurements (mean ± SD). Lime-treated samples were sealed in airtight double plastic bags and tested within 24 h to minimize carbonation.

2.2.2. Sample Preparation and Testing Program

The Mershon kaolin soil was dried in an oven at 105 °C for about 24 hours. Then, the dry kaolin soil was passed through sieve No. 4 (4.76 mm) to remove any coarse aggregates. The kaolin soil was placed in airtight double plastic bags and kept under fixed laboratory conditions throughout the tests. Table 4 summarizes 15 mix designs and the corresponding number of tests performed for each mix design in this study.

Table 4 Mix designs and the number of tests have been undertaken at different curing ages

Mix design	Admixtures (wt%)				Number of tests at different curing times				
	NK	NT	MS	L	UCS	CBR	Atterberg	Compaction	pH
K	-	-	-	-	3	3	2	3	3
MS3	-	-	3	-	3	3	2	3	3
MS5	-	-	5	-	3	3	2	3	3
MS7	-	-	7	-	3	3	2	3	3
MS10	-	-	10	-	3	3	2	3	3
NT1	-	1	-	-	3	3	2	3	3
NT3	-	3	-	-	3	3	2	3	3
NT5	-	5	-	-	3	3	2	3	3
NK1	1	-	-	-	3	3	2	3	3
NK3	3	-	-	-	3	3	2	3	3
NK5	5	-	-	-	3	3	2	3	3
L3	-	-	-	3	3	3	2	3	3
L3MS7	-	-	7	3	3	3	2	3	3
L3NT3	-	3	-	3	3	3	2	3	3
L3NK3	3	-	-	3	3	3	2	3	3

The objective of designing mixes with the proposed proportions in Table 4 was primarily to improve the mechanical properties of kaolin soil while minimizing the use of admixtures. According to the literature, MS proportions of 3%, 5%, 7%, and 10% by dry weight of kaolin soil were selected [31,32]. In addition, the amount of hydrated lime was selected based on the initial consumption of lime (ICL) method introduced by Eades and Grim to increase soil alkalinity [33]. The ICL test results (Fig. 8) indicate that 3 wt% hydrated lime is required to initiate alkali reactions, per ASTM D6276 [33]. Due to the lack of comprehensive studies on kaolin soil improvement using NT and NK, the proportions of NT and NK were determined through trials to obtain an optimal value. Then, the effects of adding optimal amounts of MS, NT, and NK to the lime-treated mixes were investigated. Although optimum contents were primarily selected based on UCS performance, this choice is justified since UCS is widely recognized as the most consistent indicator of long-term pozzolanic reactivity, whereas CBR and stiffness values often exhibit greater scatter and dependency on compaction state.

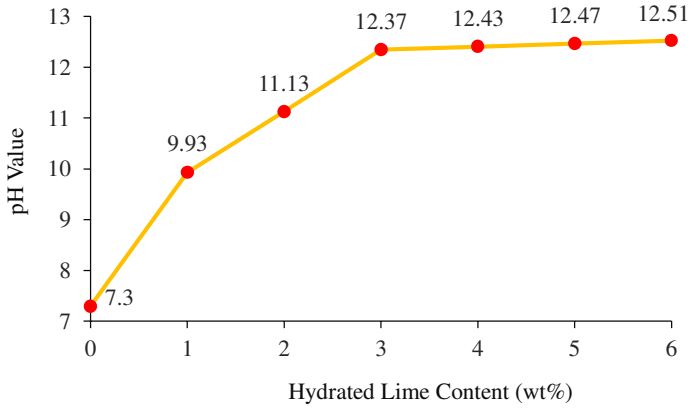


Fig. 8 Effect of hydrated lime content on pH value of lime-treated kaolin soil

To ensure uniformity in the mixture, NT and NK powders, along with distilled water, were sonicated at room temperature in a container for three sets of 15 minutes each before adding them to the kaolin soil. Then, an automatic soil mixer was used to mix the kaolin soil with the admixtures for about 10 minutes. The homogeneity of the mixtures was visually inspected until the appropriate mix was achieved.

The Atterberg limits test was conducted according to the standard procedure described in ASTM D4318 [26]. The liquid limit (LL), plastic limit (PL), and plasticity index (PI) were determined for each mix design. The experiment was replicated, and the average values for each mix design were reported to obtain more reliable results. The compaction properties of each mix design, including the optimum moisture content (OMC) and maximum dry density (MDD), were determined using the standard Proctor test method, as specified in ASTM D698 [27]. The compaction tests for each mix design were repeated three times, and the average values were reported by considering the standard deviation. In addition, the UCS tests were conducted on untreated and treated mixes in accordance with ASTM D2166 [30]. The failure peaks for each sample were measured on a hydraulic testing machine at a loading rate of 0.95 mm/min (≈1.25% axial strain/min). The load cell had a capacity of 1 ton, and the results were reported with a resolution of 0.01. The acquisition data unit automatically recorded the applied load and the axial deformation. The failure of each sample was defined by its peak axial stress. In addition, the loading platens were lubricated to minimize end friction. The specimens should comply with the following maximum errors: ±0.5 mm for the diameter, ±2 mm for the height, ±1% for the dry unit weight, and ±0.5% for the moisture content.

The UCS samples were prepared at target OMC and MDD values, obtained from standard Proctor tests. In this regard, water was gradually added to the mixtures until OMC values were achieved. Furthermore, the compaction at the target dry density was obtained by compressing the mixture in a steel cylindrical mold using a hydraulic jack, in accordance with BS 1924-2 [34]. Finally, the cylindrical samples were extruded using a steel plunger, trimmed to be parallel and flat, and sealed in double-layered plastic bags (no capping was used for specimens). The size of specimens measured 35 mm in diameter and 76 ± 2 mm in length. These samples were cured for 3, 7, and 28 days in a temperature-controlled room (25 ± 2 $^{\circ}$C, 85% humidity) before conducting the UCS testing. Three parallel samples were made for each mix design group to improve the reliability of UCS test results. Then, the average value was used in the report by considering the standard deviation. In total, 135 samples were fabricated for the UCS experiment. Moisture content and dry density of representative specimens were verified after curing, showing deviations within ±1% of target values.

The soaked CBR tests were conducted for each mix design to evaluate the bearing capacity of untreated and treated mixes, according to ASTM D1883 [35]. CBR specimens, with diameters of 152 mm and heights of 127 mm, were compacted to their OMC and MDD using the same method as for the UCS samples. Then, the CBR specimens were cured under the same conditions as the UCS samples (25 ± 2 $^{\circ}$C, 85% humidity) to ensure consistent results. Before penetration testing for the soaked condition, the specimens were submerged in water for 96 hours. CBR tests were conducted on 15 mix designs at 4, 7, and 28 days of curing. Following ASTM D1883 [35], CBR was determined at penetration depths of 0.1 in. (2.5 mm) and 0.2 in. (5 mm), and the higher value was adopted as the final CBR, consistent with the standard practice. To obtain convergent results, each CBR test was repeated three times, and the average

values were reported by considering the standard deviation. The strain rate during the CBR test was set at 1.27 mm/min.

2.2.3. Reliability of Measurements

Each experiment was repeated at least 2 or 3 times, depending on the test type, to ensure the accuracy of the results. The number of replications (N) for each test is summarized in Table 5. The acceptable standard deviation (SD) for each test was determined based on relevant standards and previous studies. The mean standard deviations and coefficients of variation (CV) obtained from the present study indicate that the results fall within the acceptable limits of repeatability reported in the literature.

Table 5 Reliability measurements of tests

Tests	Properties/Curing days	N	Acceptable SD	Mean SD	Mean CV (%)
Atterberg limits	PL (%)	2	2	1.0	3.6
	LL (%)	2	2	1.2	2.9
	PI (%)	2	2	1.3	7.2
Compaction	OMC (%)	3	0.3	0.15	1.25
	MDD (g/cm^3)	3	0.02	0.008	0.42
UCS (kPa)	3d	3	0.1	0.05	5
	7d	3	0.1	0.08	6.7
	28d	3	0.1	0.07	4.7
CBR (%)	4d	3	1	0.6	6
	7d	3	1	0.9	6.9
	28d	3	1	0.5	2.5
pH	0d	3	0.05	0.03	0.3
	7d	3	0.05	0.03	0.3
	28d	3	0.05	0.03	0.3

2.2.4. Finite Element Modeling (FEM)

A numerical assessment was conducted to evaluate the performance of sealed roads stabilized with optimal amounts of MS, NT, and NK, with and without 3 wt% hydrated lime. The vertical deformation and response of stabilized sealed roads were studied under static traffic load. The finite element analysis was performed using PLAXIS 2D version 2024.3. PLAXIS 2D is a finite element package used to analyze the deformation, stress-strain, and stability of geotechnical infrastructures, including various pavements. Figure 9 shows the cross-section geometry for the pavement analysis.

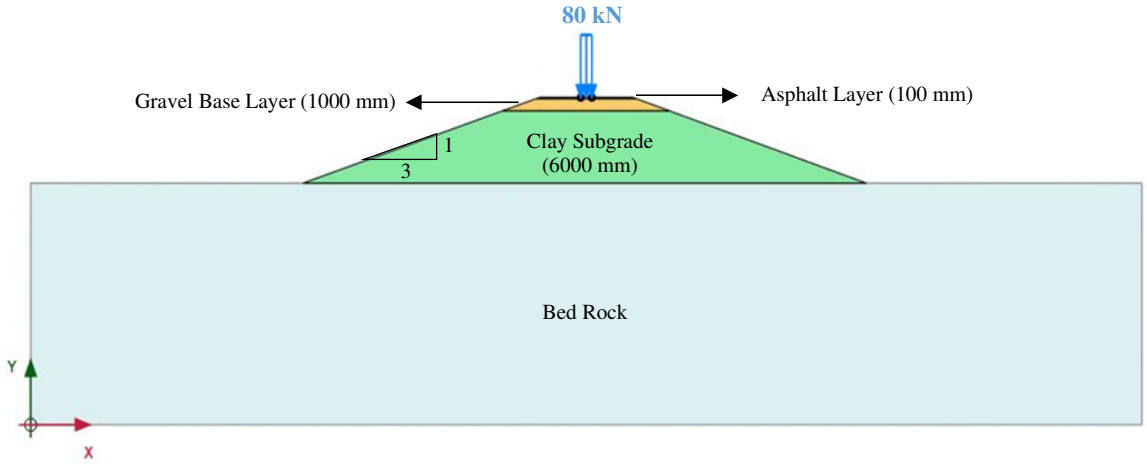


Fig. 9 Cross-section of the pavement layers and distributed loading

The simple pavement with a 3:1 slope consists of three layers, including a bituminous asphalt surface layer (100 mm), a gravel base layer (1000 mm), and a clay subgrade layer (6000 mm). The asphalt layer was modeled as a Linear Elastic material, whereas the base and subgrade were modeled using the Mohr-Coulomb model. Furthermore, the interfaces between layers are considered fully bonded (no gaps). After conducting a series of sensitivity analyses, a plane-strain model was employed, using 15-node structural solid elements with fine refinement. The Equivalent Standard Axles (ESA) was assumed to be 1×10^7, and the static 80 kN single-axle-dual-tyre (SADT) loading was uniformly applied to an equivalent circular area (contact area radius = 0.11 m) of the top layer [40,41]. In addition, the allowable vertical strains for a presumed ESA of 1×10^7 road pavement is restricted to 915 με, based on the equation stated in section 5.8 of Austroads guideline [40]. The equation for the limiting strain criterion is presented as follows:

$$N = \left[\frac{9150}{\mu\varepsilon}\right]^2 \quad (1)$$

where,

N: the allowable number of repetitions of a Standard Axle at this strain before an unacceptable level of pavement surface deformation develops (units of ESAs),

με: the vertical compressive strain (in terms of microstrain), developed under a Standard Axle, at the top of the subgrade.

Further, soil boundaries were assumed to be located far from traffic loads to eliminate boundary effects. The vertical and horizontal displacements at the surface were allowed, while the bottom of the model was fully fixed and horizontally restrained at extremes. In addition, the drainage system was assumed to be adequate so that the effects of water on pavement design were omitted from the analysis.

2.2.5. Pavement Properties

In this study, a conventional urban road consisting of bounded granular pavements with a thin bituminous surfacing was simulated in accordance with Austroads' empirical design guidelines [40]. The assumed roadway consisted of two lanes with a lane width of 4.2 m and a subgrade depth of 6 m. The typical CBR values for the subgrade with CL soil type and an

excellent to good drainage system should be in the range of 5 to 6, according to Austroads manual guidelines [40]. However, the CBR value obtained for kaolin soil in this study is 3, indicating that this soil is not suitable for the subgrade layer and requires appropriate stabilization.

The mechanical properties of the soil were derived from laboratory tests conducted in this study. The cohesion (c) and internal friction angle (ϕ) were derived from the UCS test results. Considering the nature of stabilized clay soils and performing a short-term analysis, the assumption of undrained conditions was adopted for all stabilized mixtures, setting the undrained friction angle to zero ($\phi_u = 0$). Under this assumption, the undrained shear strength (cohesion, c_u) was calculated as half of the measured UCS (i.e., $c=c_u= UCS/2$).

The elastic modulus (E) required for Mohr-Coulomb Modeling was approximated by E_{50} obtained from UCS stress-strain curves (Table 5), a practice commonly adopted in numerical studies of stabilized soils [41,42]. However, the mechanical properties of the base and asphalt layers were selected based on empirical design charts [40]. In this regard, the vertical modulus and the degree of anisotropy of the base layer were assumed to be 150 MPa and 2, respectively [40]. Also, the CBR and density of the base layer were selected as 20 and 2.24 g/cm^3, respectively, based on values suggested in [42]. The elastic modulus of asphalt was assumed to be 2000 MPa, while the Poisson's ratio of all the pavement materials was taken as 0.35.

2.2.6. Analysis Plan

In the first stage, the stabilized subgrades with different mix designs were designed according to laboratory test results and empirical design charts. Then the responses of stabilized subgrades, including stresses, strains, and deformations along the surface of each layer, were evaluated. At the second stage, a parametric study was carried out to determine the minimum base thickness (t) required over the stabilized subgrade to meet the strain criteria.

2.2.7. Life Cycle Assessment (LCA)

In this section, a life cycle assessment (LCA) was employed to evaluate the environmental impacts of stabilized road pavement and compare them with those of non-stabilized road pavement. According to ISO 14040 [45] and ISO 14044 [46], the LCA comprises four phases: goal and scope definition; inventory analysis; life cycle impact assessment; and results interpretation. The LCA analyses were performed by using SimaPro software [47].

2.2.8. Goal and Scope Definition

The aim of this cradle-to-site LCA is to evaluate and compare the environmental impacts of various subgrade stabilization scenarios (MS7, NT3, NK3, L3, L3MS7, L3NT3, L3NK3) against untreated kaolin soil (K). This approach aligns with methodologies used in similar geotechnical LCA studies [47–49]. The cradle-to-site boundary was chosen because this study focuses exclusively on the environmental burdens associated with the production and delivery of stabilizing materials. This approach does not consider the entire life cycle of road construction, operation, maintenance, and end-of-life stages, which is consistent with other pavement-related LCA research [47,50]. The functional unit (FU) is defined as 1 m^2 of road with a 1 m stabilized subgrade, corresponding to 1 m^3 of treated soil. The system boundary is schematically represented in Figure 10.

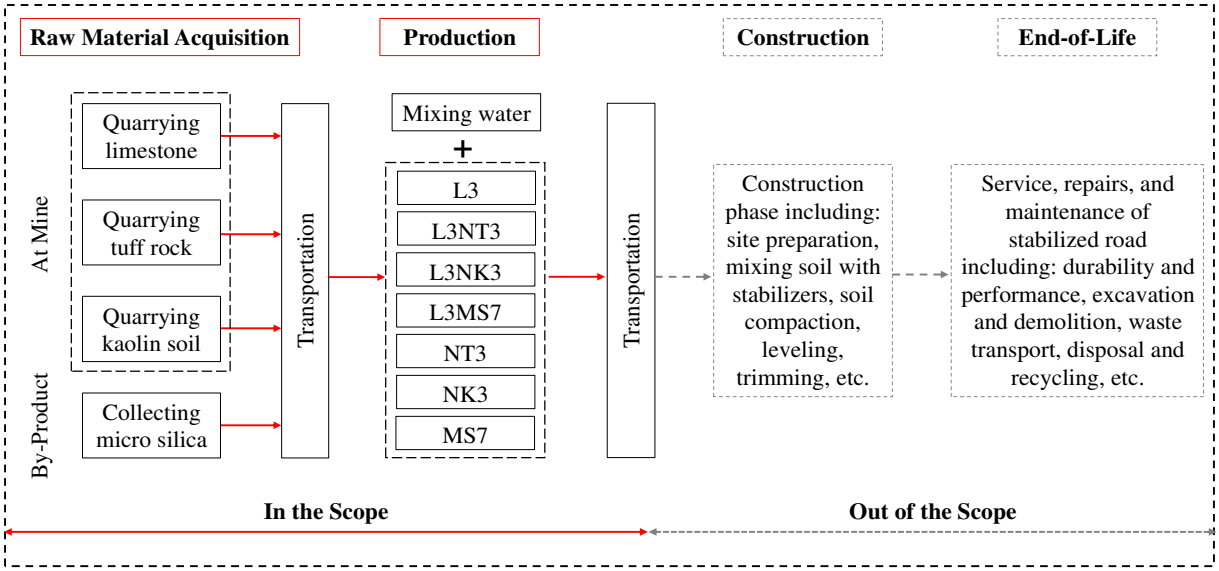


Fig. 10 Schematic diagram of system boundary and scope

2.2.9. Life Cycle Inventory (LCI) Analysis

The LCI phase quantifies all material and energy flows within the defined system boundaries (see Table 6). Inventory data were primarily sourced from the Ecoinvent 3.5 database (cut-off system model), with a focus on datasets relevant to the Iranian market. In instances where specific Iranian datasets were unavailable, we used "Global" or "Rest-of-World" equivalents. MS was treated as a cut-off by-product with zero production burden. As shown in Table 6, NT, NK, and L were represented using the relevant datasets following previous LCA studies [47,48].

Table 6 Life cycle inventory inputs for all stabilization scenarios

Mix design	Soil mass (kg)	Total mass of additives (kg)	Mixing water (kg)	Transport (t·km)	Dataset (Ecoinvent 3.5)
K	1830	—	291	0.0	—
MS7	1701.9	128.1	312	12.81	Silica fume, densified {GLO}| silica fume, densified, Recycled Content | cut-off, S
NT3	1775.1	54.9	297	5.49	Gravel, crushed, {IR}| production | cut-off, U
NK3	1775.1	54.9	296	5.49	Clay {RoW}| clay pit operation | cut-off, U
L3	1775.1	54.9	299	5.49	Lime hydrated, loose weight {IR}| cut-off, U
L3MS7	1647	183	327	18.30	Lime hydrated, loose weight {IR}| cut-off, U + Silica fume, densified {GLO}| silica fume, densified, Recycled Content | cut-off, S
L3NT3	1720.2	109.8	316	10.98	Lime hydrated, loose weight {IR}| cut-off, U + Gravel, crushed, {IR}| production | cut-off, U
L3NK3	1720.2	109.8	319	10.98	Lime hydrated, loose weight {IR}| cut-off, U + Clay {RoW}| clay pit operation | cut-off, U

Note: K = Kaolin soil; MS = Micro silica; NT = Nano tuff; NK = Nano kaolin; L = Hydrated lime

Electricity consumption for laboratory-scale ball milling of nano-materials was included for the NT3, NK3, L3NT3, and L3NK3 scenarios, calculated as 0.12 kWh/kg based on the measured 360 W power draw of the laboratory mill. The total electricity demand per FU was therefore 6.59 kWh for mixes, and the Iranian electricity mix from Ecoinvent 3.5 was applied. Transport of all materials from mine to production facilities and the construction site was fixed at 100 km, modeled using the "transport, freight, lorry, 16-32 metric ton, EURO3" dataset. This dataset represents typical supply chain distances in regional-scale projects and is applied consistently across all scenarios to ensure comparability.

2.2.10. Life Cycle Impact Assessment

The life cycle impact assessment was performed in SimaPro 9.0.0.48 using the ReCiPe 2016 Midpoint (H) method, which is widely applied in pavement and geotechnical LCA studies [47]. In this study, the following categories were selected based on their relevance to material production and transport stages: global warming potential (GWP), terrestrial acidification (TA), freshwater eutrophication (FE), marine eutrophication (ME), human non-carcinogenic toxicity (HNT), mineral resource scarcity (MRS), and fossil resource scarcity (FRS). These categories are commonly reported in similar LCA studies of soil stabilization and road material production [47–49] and provide a balanced representation of climate change, resource depletion, ecosystem health, and human health impacts.

3. Results and Discussions

3.1. Compaction Properties

Figure 11 shows the compaction variations of treated and untreated mixes. In general, increasing the amounts of MS, NT, NK, and hydrated lime in treated mixes increased OMC and decreased MDD compared to the untreated mix design. Figure 11a exhibits that adding 3, 5, 7, and 10 wt% MS to the kaolin soil increased the OMC values by 2.7%, 5.2%, 7.3%, and 10.2%, respectively, compared to the control sample. The reason for this behavior is most likely the high SSA of MS particles, which demands more water. A similar result was reported by [36], who found that adding 6 wt% MS to the kaolin soil increased the OMC by 17%. Furthermore, Figure 11a shows that adding 3, 5, 7, and 10 wt% MS to the kaolin soil decreased MDD by 1.6%, 4.3%, 6%, and 8.2%, respectively, compared to the control sample. This is mainly attributed to the lower G_s (2.20) of MS when replaced by kaolin soil with higher G_s (2.74). A similar finding was reported by Ahmadi and Shafiee [36] who noted that varying proportions of MS added to kaolin soil decreased MDD values.

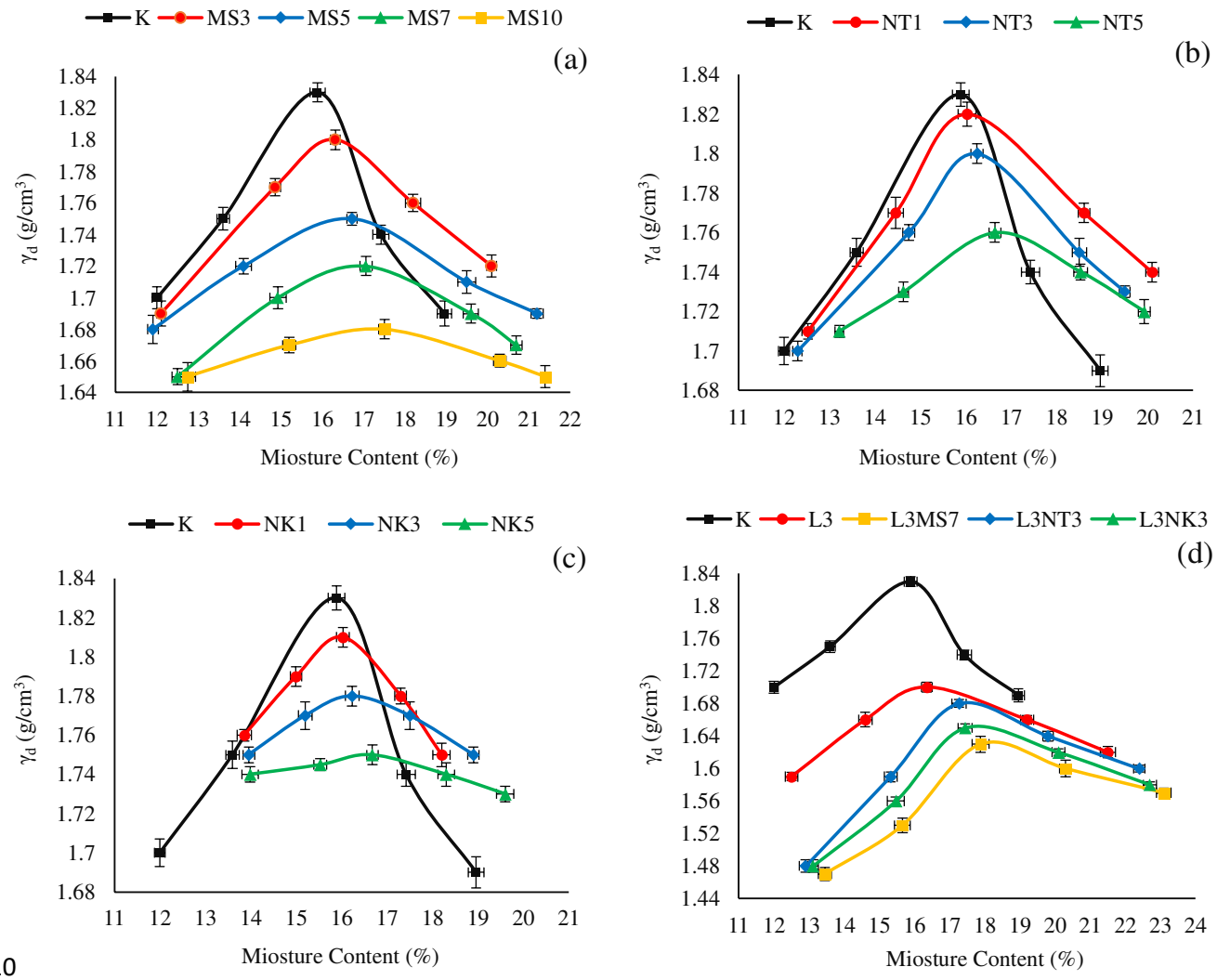


Fig. 11 Compaction properties of treated and untreated kaolin soil; a) MS, b) NT, c) NK, and d) hydrated lime-based mixtures

Figures 11b and 11c show that adding various amounts of NT and NK to kaolin soil increased OMC and decreased MDD. According to Figure 11b, adding 1, 3, and 5 wt% NT to the kaolin soil increased the OMC values by 0.8%, 2.2%, and 4.7%, respectively, compared to the control sample. Also, Figure 11c shows that adding 1, 3, and 5 wt% NK to the kaolin soil increased the OMC values by 0.8%, 2.1%, and 5%, respectively, when compared with the control sample. The high SSA and water absorption capacity of both NT and NK can explain this behavior. Their porous structure demands more water to achieve lubrication during compaction, thereby increasing the OMC. Additionally, the presence of fine reactive silica and alumina in NT and NK promotes physicochemical interactions with water molecules, further increasing moisture demand.

On the other hand, the addition of 1, 3, and 5 wt% NT to the kaolin soil decreased the MDD values by 0.5%, 1.6%, and 3.8%, respectively, in comparison with the control sample. Also, adding 1, 3, and 5 wt% NK to the kaolin soil decreased the MDD values by 1.1%, 2.7%, and 4.3%, respectively, compared to the control sample. The reduction in MDD values upon adding various proportions of NT and NK is partially due to their lower specific gravity (G_s) than that of kaolin soil. When NT and NK particles replace heavier clay particles, the overall dry unit

weight of the compacted mixtures is reduced. Moreover, the irregular morphology and porous texture of NT and NK reduce the packing efficiency of soil grains, resulting in a looser structure with lower MDD. In fact, due to the high surface activity of NT and NK, particles tend to flocculate and agglomerate, resulting in a less dense packing arrangement and, consequently, lower MDD values.

Based on the UCS test results (Section 3.3), the mix designs of MS7, NT3, and NK3, which exhibited the highest UCS values, were selected for mixing with hydrated lime-treated samples to evaluate their respective compaction properties. Figure 11d shows that adding 3 wt% hydrated lime to the kaolin soil increased the OMC by 3%, while the MDD decreased by 7.1% compared to the control sample. This increase in OMC is attributed to hydration and cation exchange reactions triggered by the addition of hydrated lime. When hydrated lime is added to the kaolin soil, calcium ions (Ca^{2+}) replace exchangeable cations on the clay surface (Mg^{2+} and alkalis), leading to flocculation and particle agglomeration. These reactions increase the demand for water to lubricate the flocculated structure and achieve maximum compaction, hence raising the OMC.

The reduction in MDD can be explained by two factors: (i) the lower specific gravity of hydrated lime (G_s = 2.40) compared to kaolin soil (G_s = 2.74), which reduces the overall dry unit weight of the mixture when a portion of clay is replaced by hydrated lime; and (ii) the formation of a more flocculated structure due to cation exchange and pozzolanic reactions, which decreases the packing density of soil grains and results in a lower MDD. These results are comparable with those obtained by Alrubaye et al. [37] for MDD and OMC trends.

A similar trend was observed in the OMC and MDD values for hydrated lime-based mixes. Specifically, the OMC values for L3NK3, L3NT3, and L3MS7 increased, while their respective MDD values decreased compared to the control sample. This can be attributed to the synergistic effect of hydrated lime with NT, NK, and MS: the high surface reactivity of these additives enhances lime-clay interactions, producing additional flocculation and agglomeration. As a result, the mixes require more water for lubrication during compaction due to higher OMC, while their dry unit weight decreases due to both the lower specific gravity of the additives and the development of a more porous microstructure due to lower MDD.

3.2. Atterberg Limits

Figure 12 illustrates the variations of Atterberg limits, including PL, LL, and PI, with the addition of different amounts of additives to the kaolin soil. Figure 12a shows that adding 3, 5, 7, and 10 wt% MS to the kaolin soil reduced the PI values by 41%, 53%, 63%, and 56%, respectively, compared to the control sample. This reduction in PI values is primarily attributed to the microfiller effect of MS and its high SSA, which reduces the proportion of active clay minerals responsible for plasticity. The replacement of clay by non-plastic MS particles decreases the adsorbed water layer and weakens the diffuse double layer around kaolinite particles, thereby lowering both LL and PI values. In other words, the ultrafine particles of MS can disperse kaolin soil grains due to their negative charge, thereby reducing PI and LL values.

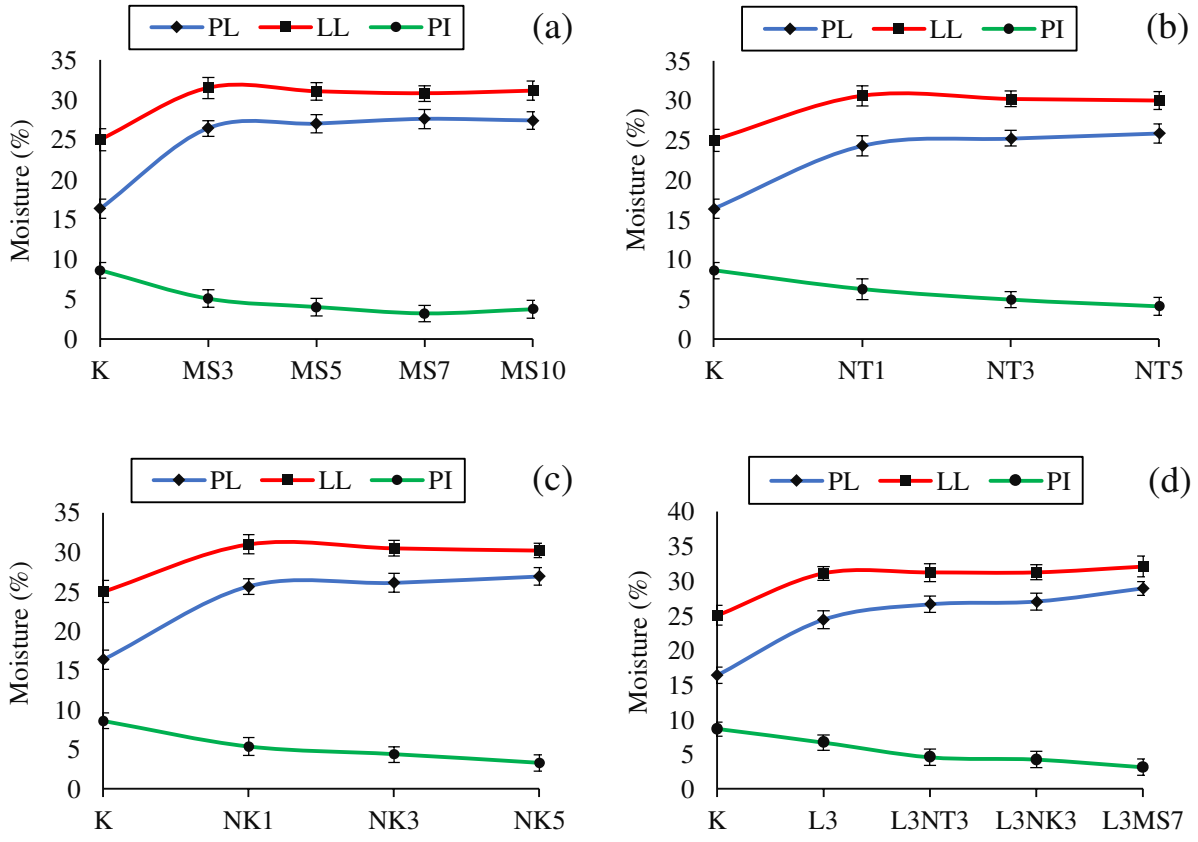


Fig. 12 Variations of Atterberg limits of treated and untreated kaolin soil; a) MS, b) NT, c) NK, and d) hydrated lime-based mixtures

Figure 12b displays that adding 1, 3, and 5 wt% NT to the kaolin soil reduced the PI values by 27, 57, and 52%, respectively, compared to the control sample. Also, Figure 12c shows that adding 1, 3, and 5 wt% NK to the kaolin soil reduced PI values by 38%, 49%, and 62%, respectively, compared to the control sample. The reduction in PI values by the addition of NT and NK can be explained by their nano-scale particle size, high surface reactivity, and strong affinity for water molecules. These characteristics promote particle flocculation and aggregation, thereby reducing the thickness of the diffuse double layer and lowering the clay's plastic deformation capacity. Moreover, replacing clay with low-plasticity NT and NK particles reduces the proportion of fines that govern plasticity, thereby decreasing LL and PI. Compared with other mix designs, NK5 shows better PI reduction performance. This can be attributed to the relatively higher surface reactivity and finer effective particle size distribution of NK compared to NT, as confirmed by the BET results in this study, and supported by Soltani et al. [9]. Thus, NK is more effective at reducing clay's plastic behavior than NT.

In addition to the individual additives, hydrated lime also reduced the PI of kaolin soil, resulting in about a 22% decrease compared to untreated soil. This reduction is mainly related to the cation exchange and flocculation mechanisms induced by calcium ions, which compress the diffuse double layer and limit the clay's plastic behavior [10]. Moreover, the lime-based combinations exhibited the most pronounced reductions in PI. Compared to the untreated soil, PI decreased by approximately 47%, 51%, and 64% for L3NT3, L3NK3, and L3MS7, respectively. The synergistic interaction between hydrated lime and the reactive silica/alumina of NT, NK, and MS enhances flocculation and pozzolanic reactions, thereby reducing the active clay fraction and plasticity. Overall, the lime-based mixes, particularly L3MS7, proved

the most effective at reducing plasticity, outperforming both the single-additive mixes and hydrated lime alone.

3.3. Unconfined Compressive Strength (UCS)

Figure 13 shows the UCS development of kaolin soil mixes when treated with different amounts of MS, NT, and NK after 3, 7, and 28 days of curing, in the presence and absence of hydrated lime.

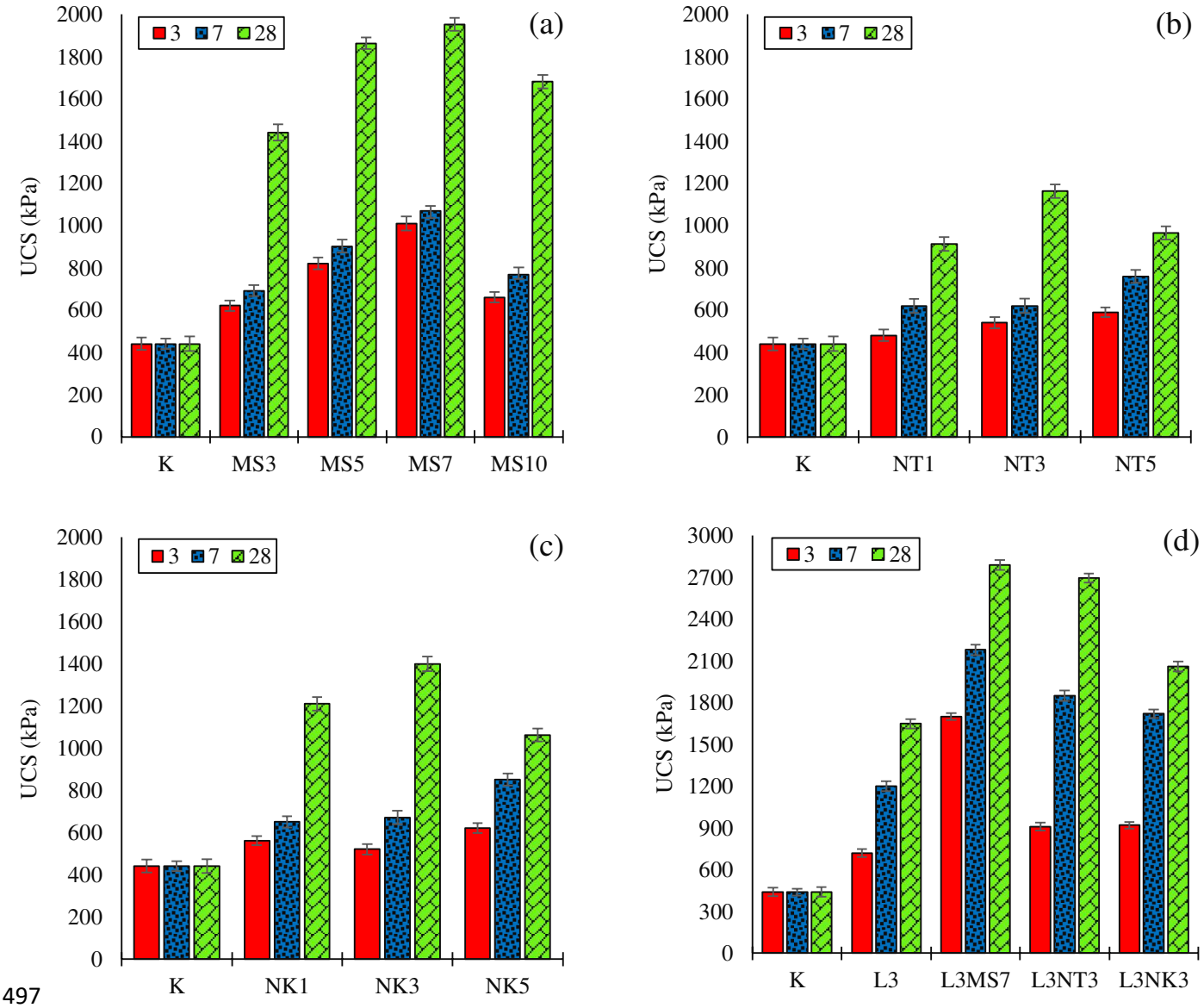


Fig. 13 UCS test results for treated and untreated kaolin soil after 3, 7, and 28 days of curing; a) MS, b) NT, c) NK, and d) hydrated lime-based mixtures

Figure 13a shows that adding 3, 5, 7, and 10 wt% MS to the kaolin soil increased the 28 day-UCS values by 3.27, 4.23, 4.43, and 3.81 times, respectively, compared to the control sample. Several researchers also reported similar improvements in UCS when MS was added to clay soils [11,37]. The enhancement in UCS is mainly due to pozzolanic reactions between the amorphous silica in MS and the activated feldspar minerals present in the kaolin soil, forming secondary cementitious products such as N-A-S-H gels. These products fill pores,

bond clay particles, and densify the soil matrix, thereby improving UCS. The highest UCS value was obtained for the MS7 mix design, while the UCS decreased at MS10. This reduction is likely due to excessive replacement of clay with non-cohesive MS particles, which reduces particle-particle bonding and results in weaker soil structure at higher replacement levels.

Figure 13b demonstrates that adding NT to the kaolin soil also increased UCS over longer curing times. Adding 1, 3, and 5 wt% NT improved the 28-day UCS values by 2.06, 2.63, and 2.15 times, respectively, compared to the control sample. The UCS trend shows that NT3 was the strongest mix design compared with NT1 and NT5. The UCS improvement in NT-treated mixes can be explained by the high reactivity and large SSA of NT particles, which enhance flocculation of clay minerals and accelerate pozzolanic reactions. NT contributes reactive silica and alumina, which interact with the clay matrix to form cementitious compounds that bind particles more effectively. The decrease at higher replacement (NT5) indicates that excessive NT addition disturbs the soil structure and reduces effective bonding.

Figure 13c illustrates the UCS results for the NK-treated mixes. The addition of 1, 3, and 5 wt% NK to kaolin soil resulted in UCS increases of 2.41, 3.15, and 2.72 times, respectively, compared to the control sample after 28 days. A similar trend has been reported by other researchers using nano-kaolinite [38]. The improvement is mainly due to the NK particles, which provide nucleation sites for hydration and pozzolanic reactions, enhancing the bonding of soil particles. NK also improves soil structure by filling micropores and strengthening the clay matrix. Optimum performance was observed for NK3, whereas NK5 showed reduced UCS values. This reduction is most likely caused by particle agglomeration at higher NK contents, which reduces the effective reactive surface area and creates weak zones in the compacted soil.

Figure 13d shows the UCS development of mixes containing 3 wt% hydrated lime added to the optimum designs (MS7, NT3, and NK3). The 28 day-UCS increased by 6.33, 6.12, and 4.67 times, respectively, compared to the control sample. Adding 3 wt% hydrated lime to kaolin soil alone increased UCS by 3.74 times. The strength improvement in lime-treated mixes is attributed to cation exchange, flocculation, and the formation of cementitious compounds (C-A-S-H and N-A-S-H) through pozzolanic reactions between hydrated lime and clay minerals. Furthermore, the combination of hydrated lime with silica/alumina-rich additives (MS, NT, and NK) enhances these pozzolanic reactions, providing additional nucleation sites and reactive surfaces for gel formation. This synergistic effect results in significantly higher UCS values, particularly at longer curing times.

3.4. Failure Strain and Modulus of Elasticity

Table 7 presents the failure strains (ε_{50}) and corresponding modulus of elasticity (E_{50}) of all mixes after 28 days. E_{50} was obtained as the secant modulus at 50% of peak axial stress from the UCS stress-strain curve. Results show that E_{50} values generally increased with the addition of additives and with curing time, due to the formation of cementitious products (C-A-S-H and N-A-S-H gels) and the densification of the soil structure. Among single-additive mixes, MS7 achieved the highest stiffness (about 2.9 times higher than the control sample), mainly because of the high pozzolanic reactivity and micro-filler effect of MS (Fig. 14). The effect was more pronounced for lime-treated mixes (Fig. 15), where adding 3 wt% hydrated lime to kaolin soil increased E_{50} by 12.5 times, while the L3NK3 showed the most significant improvement (about 14.5 times). This highlights the synergistic interaction between hydrated

lime and the additives, which provides additional reactive surfaces for pozzolanic reactions and significantly enhances stiffness over prolonged curing.

Table 7 Stress-strain results for mixes cured until 28 days

No.	Mix design	Failure strain (ε_{50}, %)	Secant stress at 50% of peak UCS (kPa)	E_{50} (MPa)
1	K	1.77	220.34	12.44
2	MS3	2.21	721.17	32.63
3	MS5	2.86	932.27	32.59
4	MS7	2.71	976.50	36.03
5	MS10	2.53	591.18	23.36
6	NT1	2.01	457.03	22.73
7	NT3	1.82	581.82	31.96
8	NT5	2.26	483.03	21.37
9	NK1	2.90	604.70	20.85
10	NK3	2.39	699.33	29.26
11	NK5	1.56	530.86	34.03
12	L3	0.53	824.35	155.53
13	L3MS7	0.82	1394.50	170.06
14	L3NT3	1.12	1348.23	120.37
15	L3NK3	0.57	1030.00	180.70

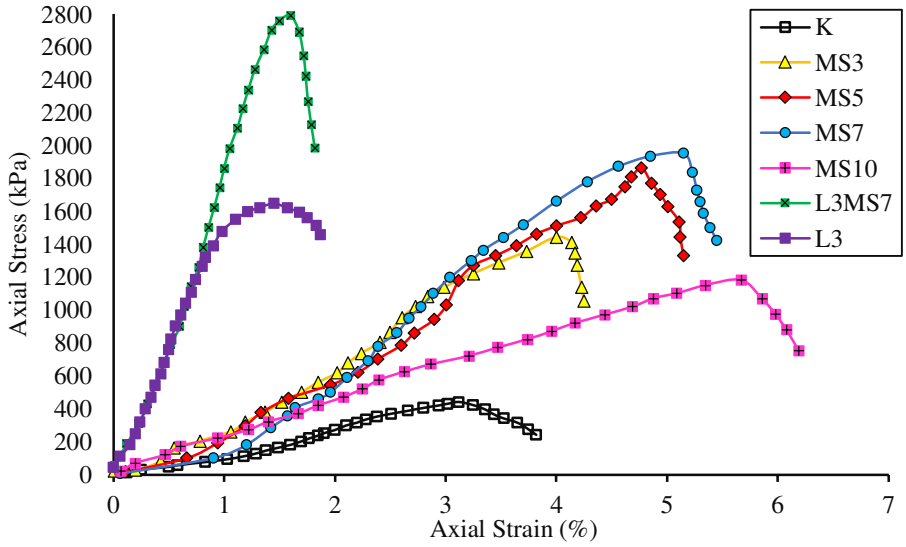


Fig. 14 Stress-Strain curve for MS-treated mixes with and without hydrated lime cured until 28 days

In terms of ductility, failure strains of MS- and NT-treated mixes increased with additive content, indicating more ductile flocculated structures (see Figs. 14 and 15). Conversely, NK-treated mixes showed reduced failure strain at higher contents (Fig. 16), most likely due to particle agglomeration forming denser and less deformable structure. The incorporation of hydrated lime, however, markedly decreased failure strains (about 70% for hydrated lime alone, 53% for L3MS7, 37% for L3NT3, and 68% for L3NK3), reflecting a transition toward brittle behavior. This fragility is consistent with the stronger cementitious bonding induced by hydrated lime-additive interactions, as also reported in previous studies [10,37].

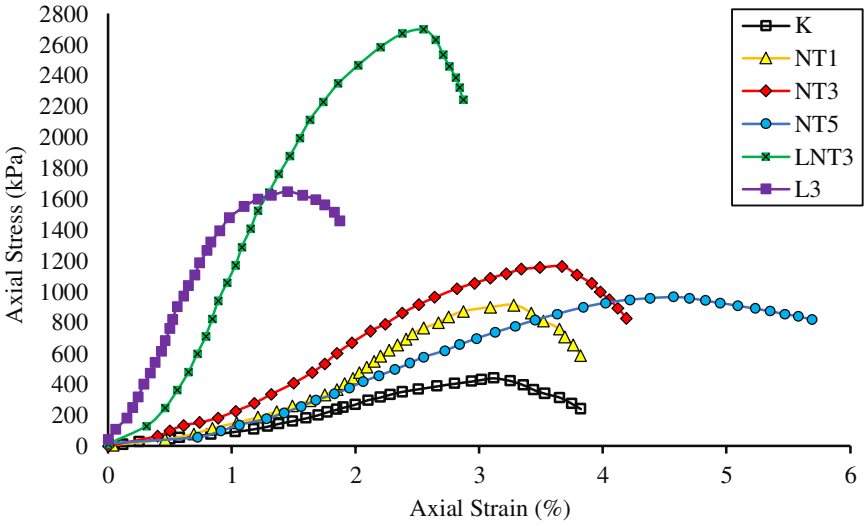


Fig. 15 Stress-Strain curve for NT-treated mixes with and without hydrated lime, cured until 28 days

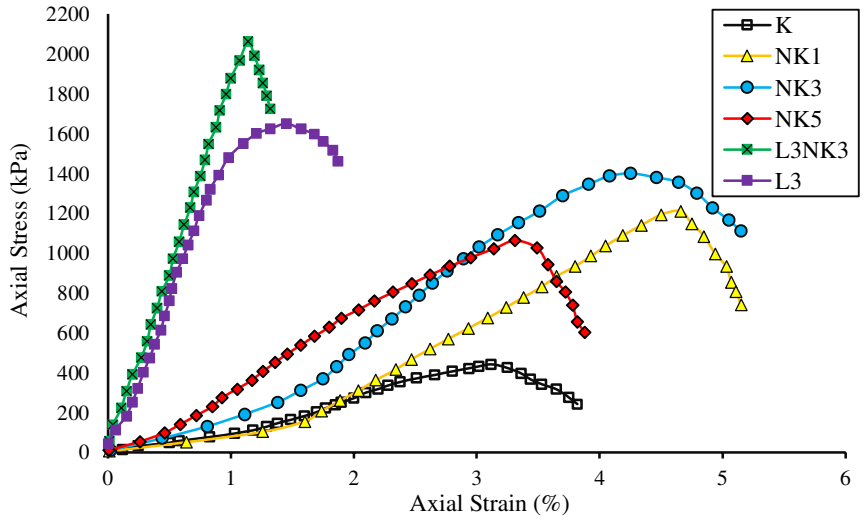


Fig. 16 Stress-Strain curve for NK-treated mixes with and without hydrated lime, cured until 28 days

3.5. California Bearing Ratio (CBR)

Figure 17 illustrates the variations of soaked CBR values for different mix designs cured for 4, 7, and 28 days [35]. It can be observed that the CBR value of treated kaolin soil increased with the addition of MS, NT, and NK, with or without hydrated lime, and further improved with longer curing time.

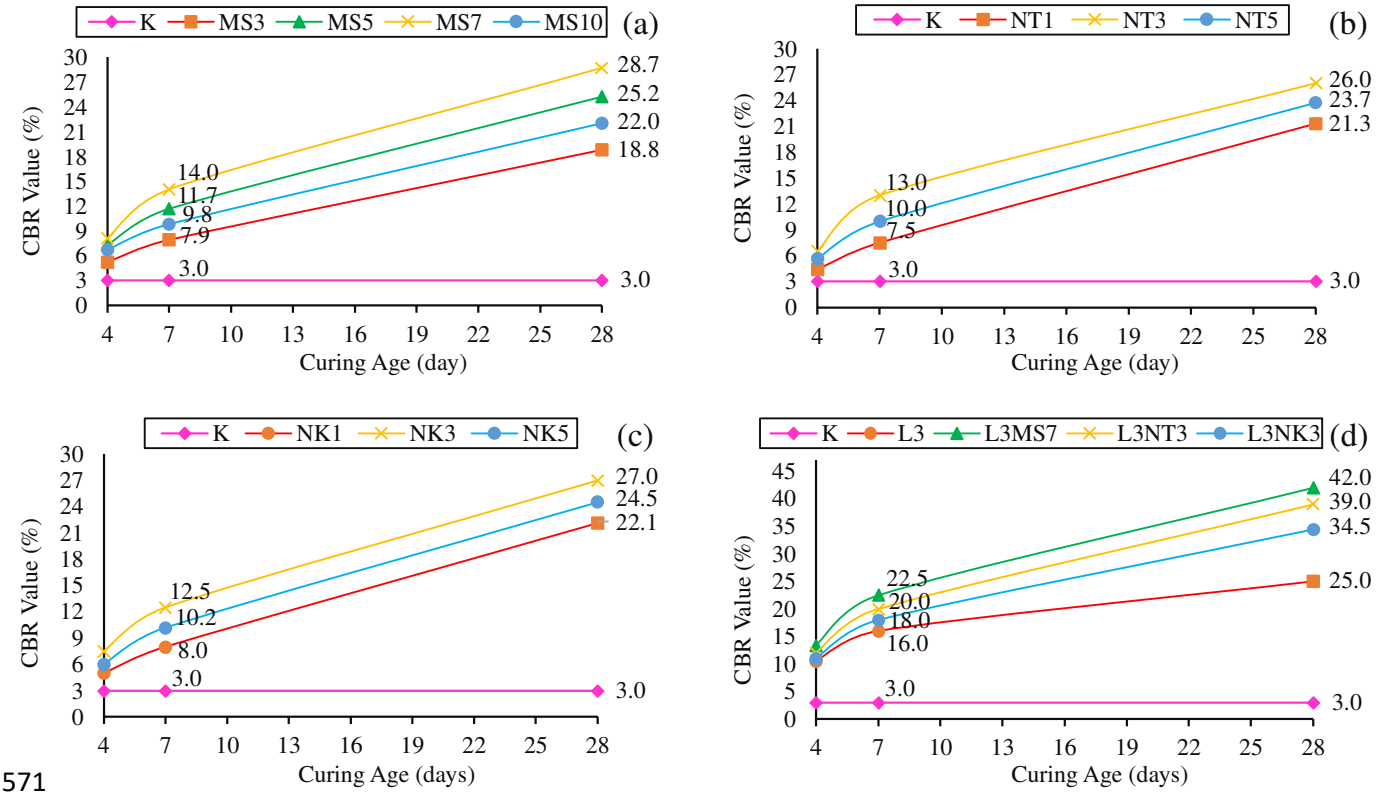


Fig. 17 Variations of CBR values for treated and untreated kaolin soil mixes cured until 4, 7 and 28 days; a) MS, b) NT, c) NK, and d) hydrated lime-based mixes

Figure 17a shows that increasing the MS content to 7 wt% and curing for 28 days resulted in the highest CBR values, whereas MS10 led to a reduction. The improvement is mainly attributed to the filler effect and high silica content of MS, enhancing textural soil matrix by densification. However, excessive MS addition reduces the proportion of clay fraction needed for cohesion, leading to a decline in CBR.

Figure 17b depicts that NT addition also improved CBR, with NT3 giving the best performance after 28 days. The increase is due to NT's high surface activity, which accelerates pozzolanic reactions and improves interparticle bonding. At higher content (NT5), particle agglomeration reduces the effective reactive surface, resulting in lower strength.

Similarly, Figure 17c shows that NK-treated mixes exhibited increasing CBR values up to 3 wt% addition, after which the values declined. The superior performance of NK compared to NT is associated with its finer effective particle size and higher surface reactivity, which provide more nucleation sites for pozzolanic products and better interlocking between soil particles. However, at NK5, excessive agglomeration reduces efficiency, decreasing the CBR values.

The most significant CBR improvements were observed in lime-treated mixes (Fig. 17d). Adding 3 wt% hydrated lime to kaolin soil alone increased CBR substantially due to cation exchange, flocculation, and the formation of C-A-S-H and N-A-S-H gels that improve strength and stiffness. The highest CBR values after 28 days were obtained for L3MS7 (42%), L3NT3 (39%), and L3NK3 (34.5%). These increases demonstrate the synergistic effect of hydrated lime with MS, NT, and NK, in which reactive silica and alumina from the additives enhance

pozzolanic activity, resulting in much higher bearing capacity than either hydrated lime or the additives alone.

Overall, the results indicate that while each additive alone improved CBR, the lime-based mixes, particularly L3MS7, achieved the highest bearing capacity after 28 days, confirming the effectiveness of combined stabilization.

3.6. pH Measurements

Figures 18 and 19 show the variations in pH levels of mixes containing different amounts of L, MS, NT, and NK at curing ages of 0, 7, and 28 days. It was observed that pH values increased with the addition of L, MS, NT, and NK to the approximately neutral kaolin soil (pH = 7.3). According to Figure 18, the highest pH evolution among the single-additive mixes (from 7.3 to 9.4) was observed with NT3, which is mainly attributed to the inherently higher alkalinity of NT compared with MS and NK (Table 3). However, the most significant pH developments were observed in lime-treated mixes. Figure 19 shows that adding 3 wt% hydrated lime to kaolin soil raised the pH from 7.3 to 12.3, while the combinations of L3MS7, L3NT3, and L3NK3 reached pH levels of 12.1, 12.2, and 12.0, respectively. Such a highly alkaline environment is essential for dissolving silica and alumina from clay particles and alumino-silicate additives, thereby promoting the formation of cementitious products (C-A-S-H and N-A-S-H gels).

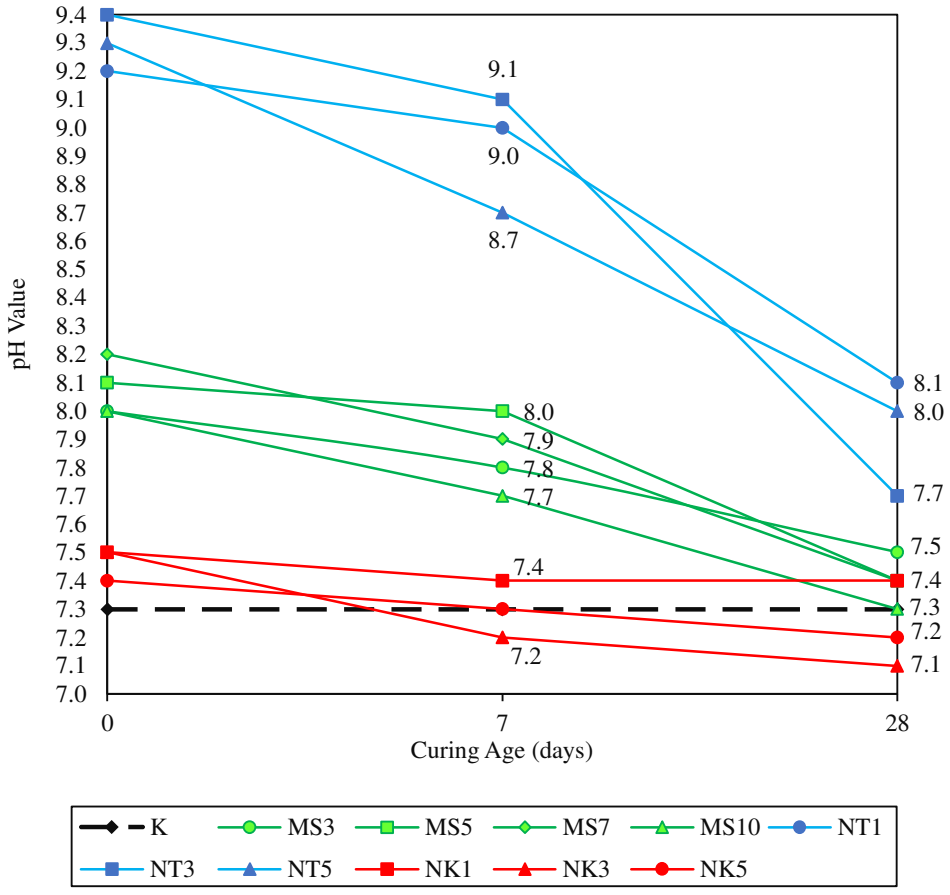


Fig. 18 Variations of pH for kaolin soil mixes treated with different amounts of NT, MS, and NK after 1 hour, 7 days and 28 days of curing

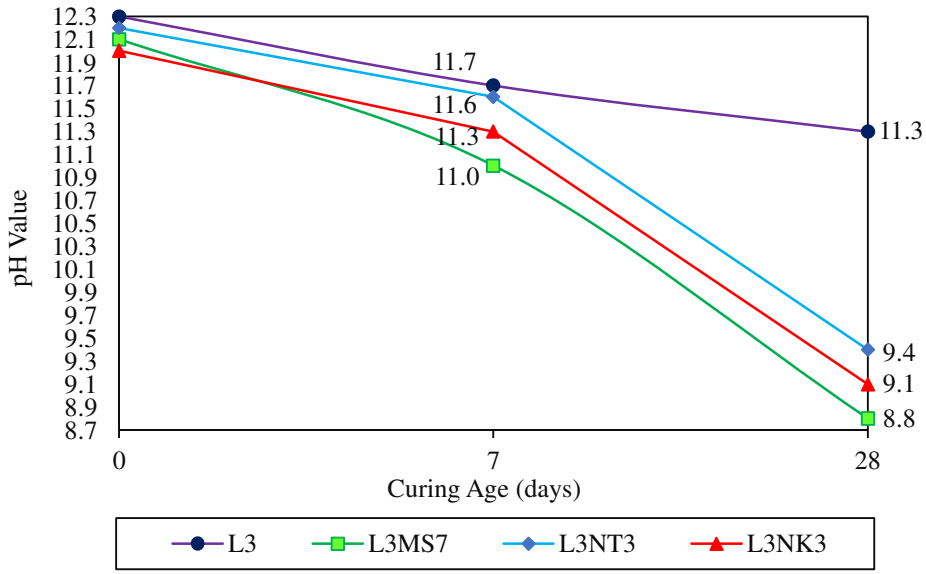


Fig. 19 Variations of pH for kaolin soil mixes treated with combinations of 3 wt% hydrated lime and various amounts of additives after 1 hour, 7 days and 28 days of curing

Over time, pH values decreased for all mixes. For MS, NT, and NK (without hydrated lime), the reduction is most likely caused by alkali exchange between the additive particles and clay minerals, which gradually neutralizes the pore water environment. For lime-treated mixes, the main cause of pH reduction is the consumption of free $Ca(OH)_2$ during pozzolanic reactions. As Ca^{2+} and OH^- ions are progressively consumed to form cementitious compounds, the concentration of hydroxyl ions in pore water decreases, leading to a reduction in pH. Nevertheless, pozzolanic reactions continue as long as the pore solution maintains a pH above 10, which was the case in all lime-treated mixes throughout the curing period.

The most significant pH reduction (from 12.1 to 8.8) was observed in the L3MS7 mix design after 28 days (Fig. 19), suggesting that MS particles exhibit slightly higher pozzolanic activity than NT and NK by consuming a larger amount of $Ca(OH)_2$. This highlights the strong reactivity of MS in alkaline environments, which contributes to the enhanced strength and stiffness observed in previous sections (Sections 3.3 to 3.5).

3.7. Mineralogical and Morphological Characterization of Stabilized Clay Soil

3.7.1. X-Ray Diffraction (XRD)

The mineralogy of selected treated kaolin soil mixes cured for 28 days was analyzed by XRD, and the results are shown in Figure 20.

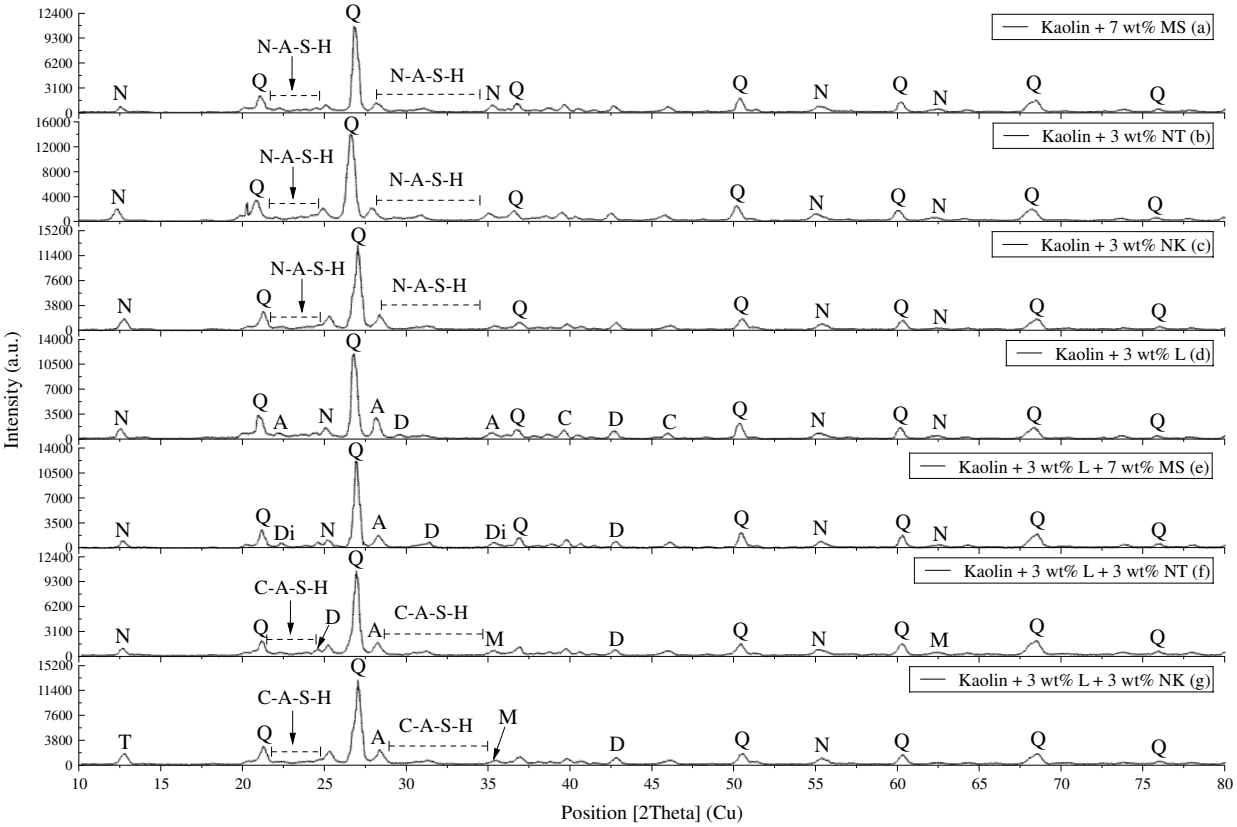


Fig. 20 XRD pattern for treated kaolin soil mixes after 28 days of curing; a) MS7, b) NT3, c) NK3, d) L3, e) L3MS7, f) L3NT3, g) L3NK3

Figure 20a shows that adding 7 wt% MS to kaolin soil revealed crystalline phases and amorphous features after 28 days. The major peak at 2θ = 26.8° corresponds to quartz. Furthermore, a broad hump between 2θ = 21.5°-24.8° and 28°-35° was observed, characteristic of the formation of an amorphous N-A-S-H (sodium aluminosilicate hydrate) gel. As reported by Garcia-Lodeiro et al. [39], in low-calcium environments, ion exchange between clay minerals and aluminosilicate sources promotes the formation of stable amorphous N-A-S-H gel. This gel contributes significantly to the strength and stiffness improvements observed in MS-treated mixes. In addition, nacrite, a polymorph of kaolinite, was also identified at 2θ = 12.5°, 25.1°, 35.2°, and 55.3°, indicating structural transformation of the kaolin soil into a more stable crystalline phase.

Figures 20b and 20c present the XRD results of NT3 and NK3 mixes. Similar to MS7, the main crystalline phases included quartz and nacrite, with a broad hump between 2θ = 21.5°-24.8° and 28°-35°, indicative of an amorphous N-A-S-H gel. The relatively low calcium oxide contents of NT, NK, and kaolin, combined with the reduction in pH over time (Section 3.6),

created favorable conditions for N-A-S-H gel formation. The appearance of nacrite again suggests a mineralogical transition of kaolinite into a more stable crystalline form. These mineralogical changes explain the mechanical improvements observed in the UCS and CBR tests, as N-A-S-H gel enhances interparticle bonding, while nacrite formation reflects long-term stabilization.

Figure 20d shows the XRD pattern of kaolin soil treated with 3 wt% hydrated lime after 28 days. The incorporation of hydrated lime altered the crystalline phases, with new peaks corresponding to albite, nacrite, calcite, and dolomite, in addition to quartz. These phases are associated with carbonation and solid solution reactions.

Figure 20e illustrates that adding 7 wt% MS to lime-treated kaolin soil resulted in the formation of new crystalline phases, including nacrite, dolomite, albite, and possibly diaspore, while quartz remained the dominant crystalline phase. Nacrite indicates structural reorganization of kaolinite into a more stable mineral, while dolomite forms through carbonation of $Ca(OH)_2$ in the lime-rich environment (main peaks around $2\theta = 31^{\circ}$ and 42.7°). A minor peak possibly related to diaspore (α-AlO(OH)) at $2\theta = 22.2^{\circ}$ and 35.3° suggests partial transformation of alumina-rich components under alkaline conditions. Similarly, the XRD pattern of L3NT3 (Fig. 20f) showed the emergence of nacrite, dolomite, albite, and magnetite, with quartz as the major crystalline peak. The formation of nacrite again shows kaolinite stabilization, while dolomite results from the carbonation of hydrated lime. Magnetite (Fe_3O_4) likely originated from iron-bearing minerals in NT that reacted under alkaline, reducing conditions. This phase can densify the soil matrix and improve particle interlocking. Together, these phases reflect strong pozzolanic and carbonation reactions that contribute to improved long-term strength and stiffness.

The XRD results of L3NK3 (Fig. 20g) indicated the formation of both crystalline and amorphous products after 28 days. Newly detected crystalline phases included talc and magnetite, albite, and dolomite, with quartz as the dominant mineral. In addition, a broad hump between $2\theta = 21.5^{\circ}$-24.8° and 28°-35° suggested the presence of amorphous C-A-S-H (calcium silicate/aluminate hydrate) gel, confirming the synergistic role of hydrated lime and NK in producing cementitious hydrates. This is consistent with the significant UCS and CBR improvements observed for this mix design (Sections 3.3 and 3.5).

3.7.2. FE-SEM and EDX Interpretations

The FE-SEM images provide further insights into the microstructural modifications of kaolin soil treated with MS, NT, and NK at their optimum contents, with and without 3 wt% hydrated lime, after 28 days of curing.

For the MS-treated sample (Fig. 21a), the addition of 7 wt% MS resulted in significant filling of voids and a slightly packed structure of kaolin soil. The fine MS particles served as nucleation sites for N-A-S-H gel formation, which coated the surfaces of kaolinite sheets and enhanced particle bonding. In the L3MS7 mix (Fig. 21b), hydrated lime addition intensified the alkalinity of the medium, thereby accelerating pozzolanic reactions and promoting the co-existence of N-A-S-H and C-A-S-H gels. This led to a more homogeneous coverage of cloudy texture for clay particles and a denser cementitious matrix compared to MS7.

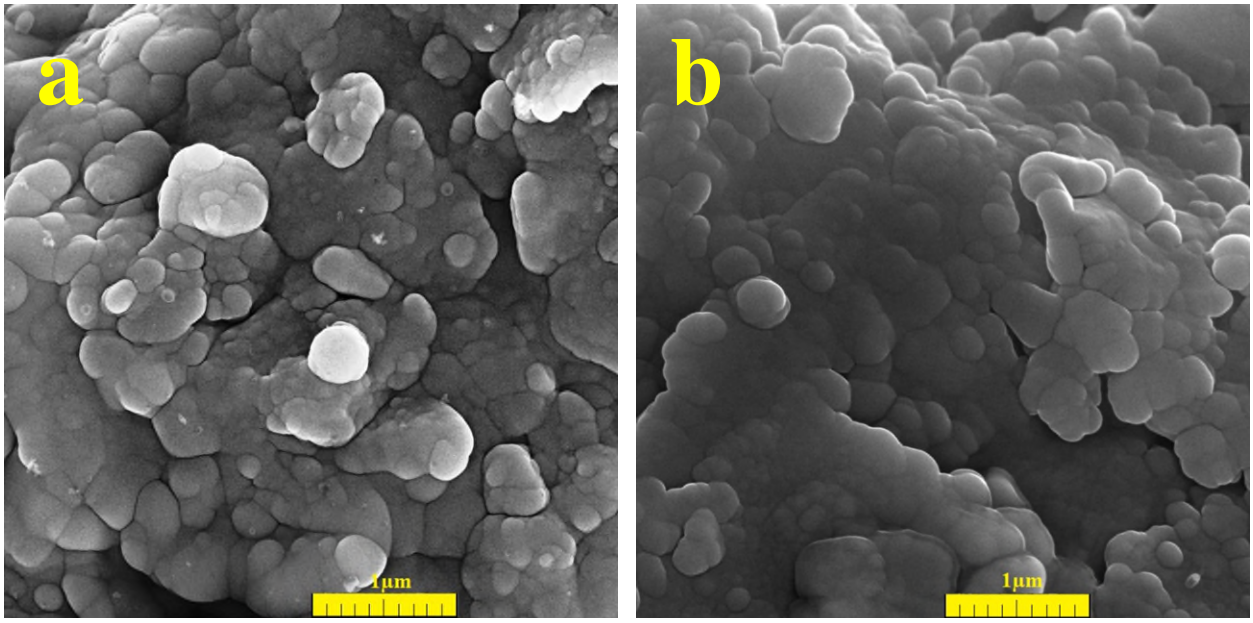


Fig. 21 FE-SEM images of kaolin soil treated with a) 7 wt% MS and b) 3 wt% hydrated lime + 7 wt% MS, cured until 28 days

690

691 For the NT-treated sample (Fig. 22a), the addition of 3 wt% NT transformed the loosely
692 packed structure of kaolin soil into a denser formation. The fine NT particles, with relatively
693 higher SSA, facilitated the formation of N-A-S-H gels and contributed to pore filling, which
694 enhanced the strength and stiffness of the soil. In the L3NT3 mix (Fig. 22b), the hydrated lime
695 addition further promoted secondary cementitious phases such as magnetite and dolomite,
696 which filled the remaining voids and created stronger particle interlinkages. This
697 microstructural densification explains the higher UCS and CBR values, as well as the slightly
698 more brittle behavior observed in mechanical tests (Section 3.4).

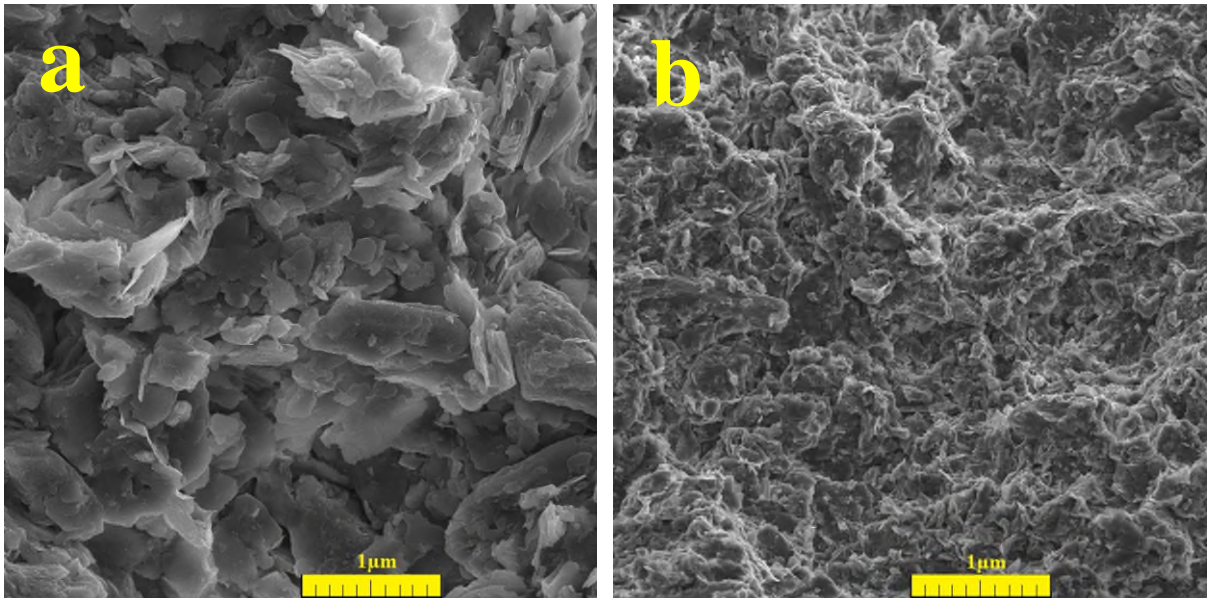


Fig. 22 FE-SEM images of kaolin soil treated mixes with a) 3 wt% NT and b) 3 wt% hydrated lime + 3 wt% NT, cured until 28 days

699

For the NK-treated sample (Fig. 23a), the incorporation of 3 wt% NK modified the porous texture of kaolin into a compacted structure by filling interparticle voids with newly formed N-A-S-H gels. The kaolinite sheets appeared more cemented together, reducing porosity and improving strength. In the L3NK3 mix (Fig. 23b), hydrated lime incorporation completely altered the texture by producing additional cementitious compounds such as C-A-S-H and magnetite, which eliminated larger voids and perfectly bonded the kaolinite sheets. The formation of a continuous cementitious network is the main reason for the superior UCS and CBR improvements observed in this mix.

In summary, the FE-SEM observations confirm that hydrated lime, when combined with aluminosilicate additives (MS, NT, NK), significantly enhanced the microstructural densification of treated kaolin soil. Among the studied mixes, L3MS7 and L3NK3 exhibited the most compact microstructures, which correlate well with the mechanical and mineralogical results.

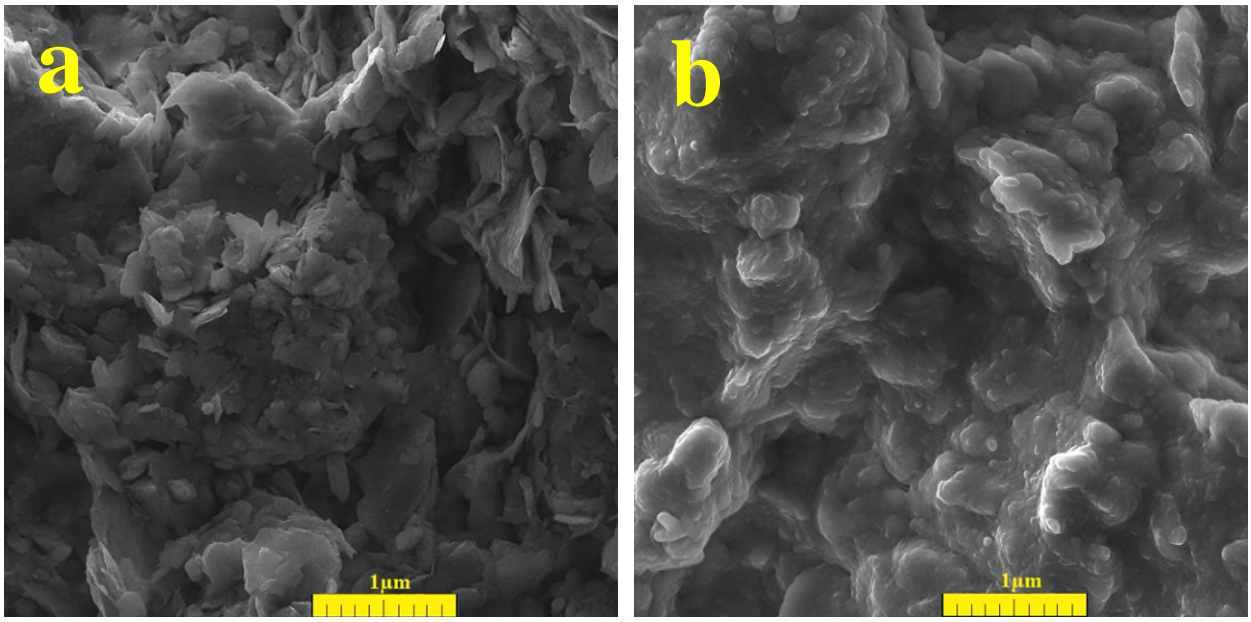


Fig. 23 FE-SEM images of kaolin soil treated mixes with a) 3 wt% NK and b) 3 wt% hydrated lime + 3 wt% NK, cured until 28 days

The EDX results at 28 days (Table 8) provide chemical evidence supporting the phase assemblages inferred from XRD and XRF. Raw kaolin soil (K) contained mainly Si and Al with very low Ca (Ca/Si = 0.008), consistent with a quartz-kaolinite system, as also indicated by the sharp quartz peak at $2\theta = 26.6^{\circ}$ in XRD and the dominance of SiO_2 and Al_2O_3 in XRF. Micro silica (MS7) was highly siliceous (Si/Al = 2.62, Ca/Si = 0.007), confirming its role as an amorphous Si source, which explains the broad amorphous hump in XRD patterns. Nano kaolin (NK3) and nano tuff (NT3) showed moderate Si/Al ratios of 2.14 and 1.90, respectively, with still negligible Ca/Si ratios (<0.02), indicating that their contribution to hydration products occurs mainly through reactive aluminosilicates. In contrast, hydrated lime (L3) displayed a significantly higher Ca/Si ratio (0.084), which is consistent with the presence of dolomite reflections in XRD and high CaO content in XRF. When hydrated lime was mixed with MS, NK, or NT (L3MS7, L3NK3, L3NT3), Ca/Si ratios markedly increased (0.098-0.192), confirming the development of C-A-S-H gels. The Si/Al values (about 1.6-2.3) suggest

coexistence of N-A-S-H and C-A-S-H phases. This interpretation agrees with FE-SEM micrographs, which show that lime-based mixes exhibit denser, more compact gel networks, while lime-free systems exhibit more porous, dispersed microstructures. Overall, the combination of XRD (amorphous hump + quartz peaks), XRF (bulk oxide composition), and EDX (atomic ratios) consistently supports the dual-gel formation mechanism: N-A-S-H dominates in lime-free systems, while C-A-S-H becomes prevalent in lime-containing mixes.

Table 8 EDX analyses of raw materials and treated kaolin soil mixes after 28 days of curing

Mix designs	O	Si	Al	Ca	K	Na	Mg	Si/Al	Ca/Si
K	53.0	26.3	15.1	0.2	1.4	3.2	0.7	1.74	0.008
MS7	55.2	28.6	10.9	0.2	1.3	3.8	0.5	2.62	0.007
NT3	55.0	25.7	13.5	0.3	1.3	3.4	0.7	1.90	0.011
NK3	54.4	27.4	12.8	0.4	1.3	2.7	0.8	2.14	0.014
L3	53.0	27.3	12.6	2.3	2.0	2.2	0.4	2.16	0.084
L3MS7	50.0	28.5	13.9	2.8	3.1	0.9	0.7	2.05	0.098
L3NT3	55.9	22.4	14.0	3.5	1.4	2.0	0.7	1.60	0.156
L3NK3	56.2	23.4	10.3	4.5	2.9	2.1	0.5	2.27	0.192

Note: Values are expressed as weight percentages (wt%), excluding H and C. The Si/Al and Ca/Si ratios are calculated on an atomic basis.

3.8. Effect of Stabilizers on Road Pavement Response

Table 9 summarizes the results of the analysis for the elastic stresses, strains, and deformations along with surface pavement layers. It shows that the elastic responses of subgrade layers stabilized with hydrated lime and additives were significantly improved compared to those of untreated kaolin soil. For example, the vertical strain at the top of the subgrade layer stabilized with MS7 decreased by 63% (from 3803 to 1384 με). Also, the vertical deformation decreased by 66% for the top layer of subgrade stabilized with the MS7 mix design.

Table 9 Critical elastic stress response due to traffic loading

Mix design	Stress (kPa)			Strain (με)			Deformation (mm)		
	Top of Surface	Top of Base	Top of Subgrade	Top of Surface	Top of Base	Top of Subgrade	Top of Surface	Top of Base	Top of Subgrade
K	79.759	69.792	55.174	640	1068	3803	32.606	32.556	30.165
MS7	79.801	74.092	57.874	112	714	1384	11.317	11.297	10.212
NT3	79.791	73.476	57.650	125	748	1555	12.990	12.985	11.710
NK3	79.795	72.989	57.685	135	774	1691	14.054	14.049	12.795
L3	79.792	78.694	61.406	39	497	335	2.981	2.977	2.374
L3MS7	79.795	78.890	61.520	36	490	305	2.716	2.713	2.024
L3NT3	79.797	78.171	60.620	45	517	430	3.695	3.692	3.044
L3NK3	79.795	78.991	61.632	35	487	287	2.594	2.594	1.936

Note: K = Kaolin soil; MS = Micro silica; NT = Nano tuff; NK = Nano kaolin; L = Hydrated lime

The elastic responses of the pavement layers further improved with the addition of hydrated lime to the kaolin soil. Specifically, the vertical strain and deformation of the lime-stabilized subgrade decreased by 91% and 92%, respectively, when compared to untreated kaolin soil. According to Table 9, the best performance for subgrade improvements was observed with the L3NK3 mix design, which resulted in a 93% reduction in vertical strain and a 94% decrease in deformation (Fig. 24). Based on the limiting strain criterion for the subgrade introduced in Austroads [40], the vertical strains for a presumed ESA of 1×10^7 should be limited to 915 με.

Therefore, the only acceptable subgrades are those stabilized with L3, L3MS7, L3NT3, and L3NK3, as they all demonstrate lower strain values (as shown in Table 9). It represents that the synergy of hydrated lime and secondary additives is necessary to improve the elastic properties of weak subgrades.

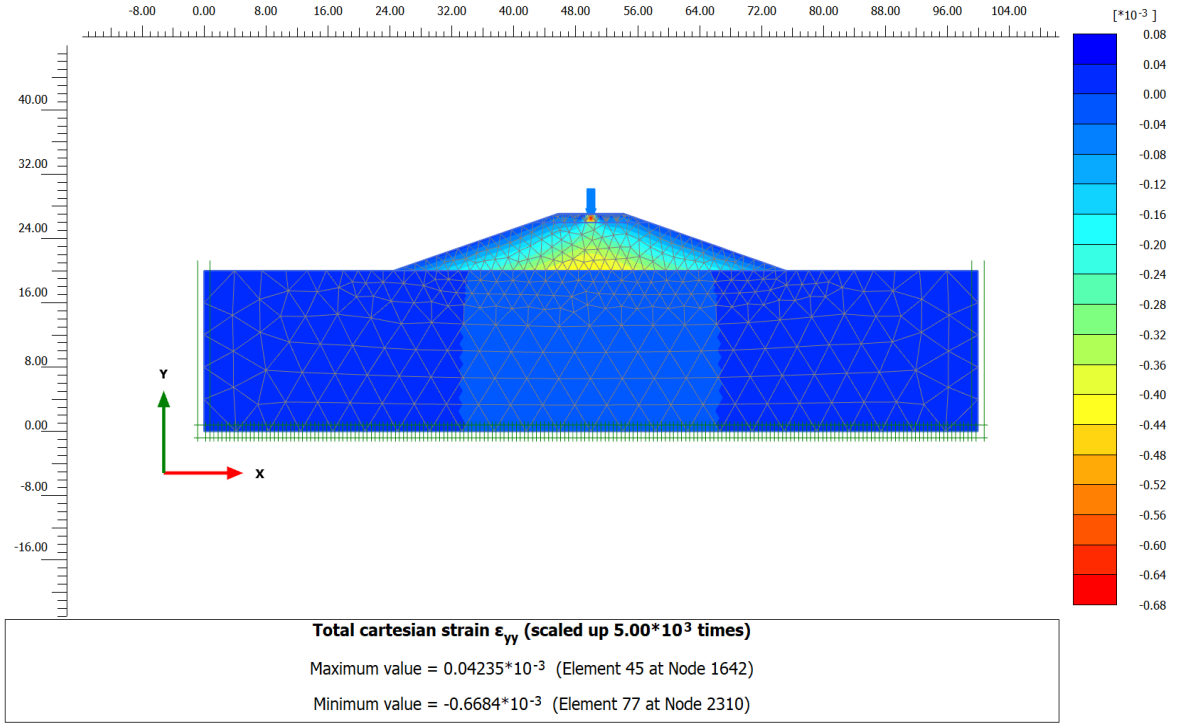


Fig. 24 Vertical strain distribution of pavement for L3NK3-stabilized subgrade

A parametric study was conducted on the stabilized and untreated pavements to evaluate the t required according to Austroads guidelines [40]. The mechanistic-empirical chart provided by Austroads indicates that the t depends on subgrade bearing capacity (CBR) and traffic loading. It was observed that a higher bearing capacity (CBR) results in a lower t when ESA remains constant. In this study, traffic loading is expressed as the design ESA (DESA), defined as the cumulative ESA carried by the design lane over the design life; accordingly, the terms ESA and DESA are used interchangeably herein. The equation for t is given by Austroads [40] as:

$$t = [219 - 211(\log \mathrm{CBR}) + 58(\log \mathrm{CBR})^2] \log(\mathrm{DESA}/120) \quad (2)$$

where,

t: minimum base thickness,

DESA: design number of ESA of traffic loading.

Consequently, a reduced t in pavement design leads to a more cost-effective and sustainable solution. In this study, as shown in Table 10, mixing additives with hydrated lime in the kaolin soil significantly reduced the t due to the improved bearing capacity of the stabilized subgrade. The reduced base thickness (Δt) values for each mix design are presented in Table 10. For example, the t in the L3MS7-stabilized subgrade was reduced by 3.3 times (from 647 to 196 mm) compared to the untreated kaolin soil subgrade, while maintaining

vertical strains within the allowable limits (915 με). This reduction is primarily attributed to the higher CBR value of the L3MS7-stabilized subgrade, which was 7.5 times higher than that of the untreated soil after 7 days. This decrease in t highlights the effectiveness of incorporating hydrated lime and secondary additives into kaolin soil, resulting in lower material needed and savings in both cost and energy for pavement projects. Similar results were reported by previous studies using hydrated lime or pozzolans for clay soil stabilization, which reduced the thickness of the base layer due to enhanced CBR values at 7 days of curing [43,44].

Table 10 Minimum base thickness (t) according to Austroads empirical chart and PLAXIS analyses

Mix design	CBR% (7-day)	t (mm)	Vertical strain (με)	Δt (mm)
K	3	647	3904	0
MS7	14	263	851	384
NT3	13	275	875	372
NK3	12.5	282	905	365
L3	16	241	386	406
L3MS7	22.5	196	348	451
L3NT3	20	210	373	437
L3NK3	18	224	378	423

Note: K = Kaolin soil; MS = Micro silica; NT = Nano tuff; NK = Nano kaolin; L = Hydrated lime

3.9. Life Cycle Assessment Results Interpretation

The LCA results (Table 11, Fig. 25) show that environmental impacts vary considerably among the stabilization scenarios. For the Climate Change indicator (GWP), which is the most critical focus of this study, lime-based scenarios demonstrate the highest impacts. This is primarily due to the calcination process, which releases large amounts of CO_2, along with the high thermal energy demand and fossil-fuel-intensive aggregate production. The lime-only scenario (L3) records a high GWP with values approximately 7.5 times higher than those of NK3 and NT3. In contrast, the nanomaterial-based scenarios without hydrated lime (NK3 and NT3) exhibit a GWP reduction of about 88% compared to the lime-based mixes (L3NK3 and L3NT3), as they circumvent calcination emissions and require smaller quantities of materials. MS7 presents the lowest GWP, mainly because MS is treated as a zero-burden by-product.

Table 11 LCA results for different mix designs and impact categories

Impact category	Unit	L3	L3MS7	L3NK3	L3NT3	MS7	NK3	NT3
GWP	kg CO_2 eq	51.03	53.20	57.40	57.57	2.61	6.79	6.97
TA	kg SO_2 eq	0.051	0.059	0.073	0.073	0.010	0.024	0.023
FE	kg P eq	0.0015	0.0017	0.0020	0.0018	0.0004	0.0007	0.0005
ME	kg N eq	0.00011	0.00013	0.00015	0.00014	0.00003	0.00005	0.00004
HNT	kg 1,4-DCB eq	3.51	4.85	5.97	4.95	1.67	2.78	1.76
MRS	kg Cu eq	0.010	0.014	0.595	0.017	0.006	0.586	0.009
FRS	kg oil eq	5.77	6.53	7.95	8.03	0.87	2.29	2.37

Note: GWP = Global warming potential; TA = Terrestrial acidification; FE = Freshwater eutrophication; ME = Marine eutrophication; HNT = Human non-carcinogenic toxicity; MRS = Mineral resource scarcity; FRS = Fossil resource scarcity

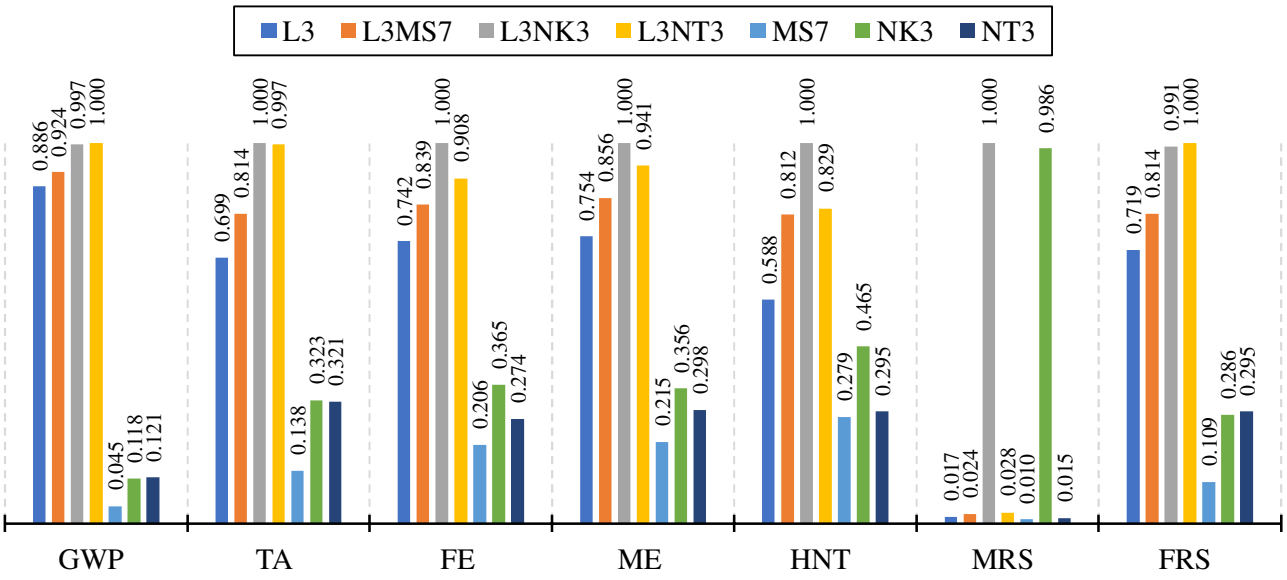


Fig. 25 Normalized LCA results to compare for different mix designs

A similar trend is observed in FRS, where L3NK3 and L3NT3 show the highest consumption of resources at over 2.6 times higher than NK3 and NT3, respectively. The lower FRS value in NK3 and NT3 mixes is linked to reduced material demand and the absence of high-temperature calcination processing. However, the electricity consumption for ball milling still contributes to their footprint, given the fossil-heavy Iranian grid mix. TA, FE, and ME potentials follow comparable patterns, with lime-based mixes consistently exceeding other mixes due to SO_2, NO_x, and phosphate emissions from limestone quarrying, calcination, and transport.

For HNT, differences between mixes are also pronounced. Lime-based mixes still show higher impacts than NK3, NT3, and MS7 mixes. For instance, the HNT value for L3NT3 is about 2.8 times higher than the NT3 mix design. This is partly due to quarrying emissions and dust, whereas nanomaterials incur additional electricity-related toxicity from milling. In MRS, lime-based mixes again dominate, with L3NT3 consuming over 1.88 times more mineral resources than NT3. It infers that the smaller mass of nanomaterial additives plays a key role in reducing impacts.

Overall, the results indicate that replacing L with NK, NT, or MS can significantly reduce environmental burdens in the production phase. This aligns with findings from similar geotechnical LCA studies [47–50], which found that high-energy calcination processes were the primary driver of impacts. However, these conclusions are subject to the study's limitations: the cradle-to-site scope excludes the use and end-of-life stages, where hydrated lime carbonation could partially offset its GWP; the fixed 100 km transport distance was applied uniformly for comparability; and electricity impacts reflect the Iranian grid mix, meaning results could change under a cleaner energy scenario.

4. Conclusions

This study evaluated the effectiveness of nano kaolin (NK) and nano tuff (NT), in comparison with micro silica (MS) and hydrated lime (L), for stabilizing low-strength kaolin

soil as a subgrade material. The experimental program, supported by microstructural analyses and finite element modeling (FEM), highlighted that the incorporation of these additives significantly enhanced the mechanical behavior of the soil. Moreover, the life cycle assessment (LCA) emphasized the importance of balancing mechanical improvements with environmental sustainability. The main findings can be summarized as follows:

- The incorporation of NT, NK, and MS notably increased UCS, CBR, and E_{50} values, particularly when combined with hydrated lime. After 28 days, L3MS7 exhibited the highest UCS improvement (6.3 times higher than the untreated clay), L3NT3 achieved its maximum CBR (39%), and L3NK3 showed the most significant stiffness increase, with E_{50} values 14.5 times higher than those of untreated clay.
- Lime-treated mixes exhibited higher stiffness but lower ductility, reflecting a transition toward more brittle failure modes.
- PLAXIS 2D analyses validated the laboratory results, showing that lime-based mixes (L3MS7, L3NT3, L3NK3) reduced vertical strains by over 90%, allowing the base course thickness to be reduced from 647 mm to 196 mm when the L3MS7 mix design was applied.
- While lime-based mixes provided the highest mechanical gains, they also carried greater environmental burdens. In contrast, NK3 and NT3 offered up to 88% lower global warming potential than L3NK3 and L3NT3, making them more sustainable alternatives.

Overall, the results highlight the promising potential of nano kaolin and nano tuff as natural supplementary additives for subgrade stabilization, offering both engineering advantages and environmental benefits for sustainable pavement applications.

Declaration of Competing Interests

The authors declare that they have no known competing financial interests or personal relationships that could have appeared to influence the work reported in this paper.

Funding Sources

This research did not receive any specific grant from funding agencies in the public, commercial, or not-for-profit sectors.

Author Contributions: CRediT

Abolfazl Soltani: Conceptualization, Supervision, Validation, Writing – review & editing. **Arash Aminaee:** Writing – original draft, Software, Methodology, Formal analysis, Visualization, Investigation, Writing – review & editing. **Atousa Alesoltan:** Methodology, Investigation, Resources. **Nabioallah Ahmadi:** Validation, Writing – review & editing. **Chinchu Cherian:** Validation, Writing – review & editing.

Data Availability Statement

The datasets analyzed during the current study are available from the corresponding author on reasonable request.

References

[1] Amakye SY, Abbey SJ, Booth CA, Mahamadu AM. Enhancing the Engineering Properties of Subgrade Materials Using Processed Waste: A Review. Geotechnics 2021;1:307–29. https://doi.org/10.3390/geotechnics1020015.

[2] Gul N, Ahmed Mir B. Performance evaluation of silty soil reinforced with glass fiber and cement kiln dust for subgrade applications. Constr Build Mater 2023;392:131943. https://doi.org/10.1016/j.conbuildmat.2023.131943.

[3] Ebailila M, Kinuthia J, Oti J, Al-Waked Q. Sulfate soil stabilisation with binary blends of lime–silica fume and lime–ground granulated blast furnace slag. Transportation Geotechnics 2022;37:100888. https://doi.org/10.1016/j.trgeo.2022.100888.

[4] Cheng Y, Wang S, Li J, Huang X, Li C, Wu J. Engineering and mineralogical properties of stabilized expansive soil compositing lime and natural pozzolans. Constr Build Mater 2018;187:1031–8. https://doi.org/10.1016/j.conbuildmat.2018.08.061.

[5] Rahman IU, Raheel M, Wajahat Ali Khawaja M, Khan R, Li J, Khan A, et al. Characterization of engineering properties of weak subgrade soils with different pozzolanic & cementitious additives. Case Studies in Construction Materials 2021;15:e00676. https://doi.org/10.1016/j.cscm.2021.e00676.

[6] Indraratna B, Korkitsuntornsan W, Nguyen TT. Influence of kaolin content on the cyclic loading response of railway subgrade. Transportation Geotechnics 2020;22:100319. https://doi.org/10.1016/j.trgeo.2020.100319.

[7] Gupta S, Kumar S. Mechanical and microstructural analysis of soft kaolin clay stabilized by GGBS and dolomite-based geopolymer. Constr Build Mater 2024;421:135702. https://doi.org/10.1016/j.conbuildmat.2024.135702.

[8] Rossato G, Ninis N, Jardine R. Properties of some kaolin-based model clay soils. Geotechnical Testing Journal 1992;15:166–79. https://doi.org/10.1520/GTJ10238J.

[9] Soltani A, Abed P, Aminaee A. Experimental studies of kaolin soil improved by calcined sepiolite as a partial replacement: mechanical performances and micro-scale analysis. Indian Geotechnical Journal 2025;55:750–65. https://doi.org/10.1007/s40098-024-00913-w.

[10] Soltani A, Aminaee A, Abed P. Improving mechanical properties of low-strength kaolin clay by mixing nano hydro carbonated shale and quicklime. International Journal of Geosynthetics and Ground Engineering 2024;10:53. https://doi.org/10.1007/s40891-024-00567-x.

[11] Zaini MSI, Hasan M, Almuaythir S, Hyodo M. Experimental investigations on physico-mechanical properties of kaolinite clay soil stabilized at optimum silica fume content using clamshell ash and lime. Sci Rep 2024;14:10995. https://doi.org/10.1038/s41598-024-61854-1.

[12] Jangde H, Khan F. Experimental investigation on interrelation between hydraulic conductivity and compressive strength of soft soil using metakaolin as stabilizer. Iranian

907 Journal of Science and Technology, Transactions of Civil Engineering 2024;48:2553–
908 65. https://doi.org/10.1007/s40996-023-01323-3.

909 [13] Dao P-L, Bui V-D, Onyelowe KC, Ebid AM, Le VD, Ahaneku IE. Effect of metakaolin
910 on the mechanical properties of lateritic soil. Geotechnical Research 2022;9:211–8.
911 https://doi.org/10.1680/jgere.22.00046.

912 [14] Badogiannis E, Kakali G, Tsivilis S. Metakaolin as supplementary cementitious
913 material. J Therm Anal Calorim 2005;81:457–62. https://doi.org/10.1007/s10973-005-
914 0806-3.

915 [15] Salimi M, Dordsheykhtorkamani A, Afrasiabian A, Khajeh A. Incorporation of volcanic
916 ash for enhanced treatment of a cement-stabilized clayey soil. Journal of Materials in
917 Civil Engineering 2021;33. https://doi.org/10.1061/(ASCE)MT.1943-5533.0003571.

918 [16] Rabab'ah SR, Taamneh MM, Abdallah HM, Nusier OK, Ibdah L. Effect of adding
919 zeolitic tuff on geotechnical properties of lime-stabilized expansive soil. KSCE Journal
920 of Civil Engineering 2021;25:4596–609. https://doi.org/10.1007/s12205-021-1603-7.

921 [17] Austroads. Guide to Pavement Technology Part 2: Pavement Structural Design. vol. 1.
922 4.4. Sydney: Austroads; 2024.

923 [18] Asadi Azadgoleh M, Mohammadi MM, AzariJafari H, Santos J, Ahmadi A, Alavi MZ,
924 et al. A comparative life cycle assessment (LCA), life cycle cost analysis (LCCA),
925 mechanical and long-term leaching evaluation of road pavement structures containing
926 multiple secondary materials. J Clean Prod 2024;458:142484.
927 https://doi.org/10.1016/j.jclepro.2024.142484.

928 [19] ASTM International. ASTM C136/C136M-19: Standard Test Method for Sieve
929 Analysis of Fine and Coarse Aggregates. vol. 04.02. West Conshohocken, PA: ASTM
930 International; 2019. https://doi.org/10.1520/C0136_C0136M-19.

931 [20] ASTM International. ASTM D7928-21: Test Method for Particle-Size Distribution
932 (Gradation) of Fine-Grained Soils Using the Sedimentation (Hydrometer) Analysis.
933 West Conshohocken, PA: ASTM International; 2021. https://doi.org/10.1520/D7928-
934 21E01.

935 [21] ASTM International. ASTM C618-22: Standard Specification for Coal Fly Ash and Raw
936 or Calcined Natural Pozzolan for Use in Concrete. vol. 04.02. West Conshohocken, PA:
937 ASTM International; 2022. https://doi.org/10.1520/C0618-22.

938 [22] ASTM International. ASTM D2487-17: Standard Practice for Classification of Soils for
939 Engineering Purposes (Unified Soil Classification System). vol. 04.08. West
940 Conshohocken, PA: ASTM International; 2025. https://doi.org/10.1520/D2487-17R25.

941 [23] ASTM International. ASTM E70-24: Standard Test Method for pH of Aqueous
942 Solutions With the Glass Electrode. West Conshohocken, PA: ASTM International;
943 2024. https://doi.org/10.1520/E0070-24.

944 [24] ASTM International. ASTM D854-23: Standard Test Methods for Specific Gravity of
945 Soil Solids by Water Displacement Method. West Conshohocken, PA: ASTM
946 International; 2023. https://doi.org/10.1520/D0854-23.

[25] International Organization for Standardization. ISO 9277:2022: Determination of the specific surface area of solids by gas adsorption — BET method. 3rd ed. Geneva: ISO; 2022.

[26] ASTM International. ASTM D4318-17e1: Standard Test Methods for Liquid Limit, Plastic Limit, and Plasticity Index of Soils. vol. 04.08. West Conshohocken, PA: ASTM International; 2017. https://doi.org/10.1520/D4318-17E01.

[27] ASTM International. ASTM D698-12: Standard Test Methods for Laboratory Compaction Characteristics of Soil Using Standard Effort (12,400 ft-lbf/ft3 (600 kN-m/m3)). vol. 04.08. West Conshohocken, PA: ASTM International; 2021. https://doi.org/10.1520/D0698-12R21.

[28] ASTM International. ASTM E1621-22: Standard Guide for Elemental Analysis by Wavelength Dispersive X-Ray Fluorescence Spectrometry. vol. 03.05. West Conshohocken, PA: ASTM International; 2022. https://doi.org/10.1520/E1621-22.

[29] International Organization for Standardization. ISO 22412:2017 Particle size analysis — Dynamic light scattering (DLS). 2nd ed. Geneva: ISO; 2017.

[30] ASTM International. ASTM D2166/D2166M-24: Standard Test Method for Unconfined Compressive Strength of Cohesive Soil. vol. 04.08. West Conshohocken, PA: ASTM International; 2024. https://doi.org/10.1520/D2166_D2166M-24.

[31] Ghavami S, Naseri H, Jahanbakhsh H, Moghadas Nejad F. The impacts of nano-SiO2 and silica fume on cement kiln dust treated soil as a sustainable cement-free stabilizer. Constr Build Mater 2021;285:122918. https://doi.org/10.1016/j.conbuildmat.2021.122918.

[32] Mousavi SE. Utilization of Silica Fume to Maximize the Filler and Pozzolanic Effects of Stabilized Soil with Cement. Geotechnical and Geological Engineering 2018;36:77–87. https://doi.org/10.1007/s10706-017-0305-x.

[33] ASTM International. ASTM D6276-19: Standard Test Method for Using pH to Estimate the Soil-Lime Proportion Requirement for Soil Stabilization. vol. 04.09. West Conshohocken, PA: ASTM International; 2019. https://doi.org/10.1520/D6276-19.

[34] British Standards Institution. BS 1924-2:2018 - TC: Hydraulically Bound and Stabilized Materials for Civil Engineering Purposes - Sample Preparation and Testing of Materials During and after Treatment. London: BSI (British Standards Institution); 2018.

[35] ASTM International. ASTM D1883-21: Standard Test Method for California Bearing Ratio (CBR) of Laboratory-Compacted Soils. West Conshohocken, PA: ASTM International; 2021. https://doi.org/10.1520/D1883-21.

[36] Ahmadi H, Shafiee O. Experimental comparative study on the performance of nano-SiO2 and microsilica in stabilization of clay. The European Physical Journal Plus 2019;134:459. https://doi.org/10.1140/epjp/i2019-12918-1.

[37] Alrubaye AJ, Hasan M, Fattah MY. Stabilization of soft kaolin clay with silica fume and lime. International Journal of Geotechnical Engineering 2017;11:90–6. https://doi.org/10.1080/19386362.2016.1187884.

[38] Abolfazl S, Maryam S, Amin M. Self-compacting soil stabilization using nano-kaolinite and OPC blends. Geotechnical and Geological Engineering 2025;43:203. https://doi.org/10.1007/s10706-025-03187-y.

[39] Garcia-Lodeiro I, Palomo A, Fernández-Jiménez A, Macphee DE. Compatibility studies between N-A-S-H and C-A-S-H gels. Study in the ternary diagram Na2O–CaO–Al2O3–SiO2–H2O. Cem Concr Res 2011;41:923–31. https://doi.org/10.1016/j.cemconres.2011.05.006.

[40] Austroads. Guide to Pavement Technology Part 2: Pavement Structural Design. vol. 1. 4.4. Sydney: Austroads; 2024.

[41] Karami H, Pooni J, Robert D, Costa S, Li Jie, Setunge Sujeeva. Use of secondary additives in fly ash based soil stabilization for soft subgrades. Transportation Geotechnics 2021;29:100585. https://doi.org/10.1016/j.trgeo.2021.100585.

[42] Jassim NW, Hassan HA, Mohammed HA, Fattah MY. Utilization of waste marble powder as sustainable stabilization materials for subgrade layer. Results in Engineering 2022;14:100436. https://doi.org/10.1016/j.rineng.2022.100436.

[43] Sambre T, Endait M, Patil S. Sustainable soil stabilization of expansive soil subgrades through lime-fly ash admixture. Discover Civil Engineering 2024;1:65. https://doi.org/10.1007/s44290-024-00063-1.

[44] Ghanizadeh AR, Salehi M, Mamou A, Koutras EI, Jalali F, Asteris PG. Investigation of Subgrade Stabilization Life-Extending Benefits in Flexible Pavements Using a Non-Linear Mechanistic-Empirical Analysis. Infrastructures (Basel) 2024;9:33. https://doi.org/10.3390/infrastructures9020033.

[45] International Organization for Standardization. ISO 14040:2006 Environmental management — Life cycle assessment — Principles and framework. 2nd ed. Geneva: ISO; 2006.

[46] International Organization for Standardization. ISO 14044:2006: Environmental management — Life cycle assessment — Requirements and guidelines. 1st ed. Geneva: ISO; 2006.

[47] Ghadir P, Zamanian M, Mahbubi-Motlagh N, Saberian M, Li J, Ranjbar N. Shear strength and life cycle assessment of volcanic ash-based geopolymer and cement stabilized soil: A comparative study. Transportation Geotechnics 2021;31:100639. https://doi.org/10.1016/j.trgeo.2021.100639.

[48] Mathankar J, Jaiswal P, Reddy S, Badiger MH. Evaluating the effectiveness of corn stalk ash as a soil stabilizer for subgrade application with emphasis on life cycle cost analysis and life cycle assessment. Innovative Infrastructure Solutions 2025;10:371. https://doi.org/10.1007/s41062-025-02180-x.

[49] Disu AA, Kolay P. Sustainability Assessment of Geopolymer Stabilized Highway Subgrades Using Industrial By-Products. Indian Geotechnical Journal 2025;55:2325–34. https://doi.org/10.1007/s40098-025-01287-3.

[50] Perri G, De Rose M, Domitrović J, Vaiana R. CO_2 Impact Analysis for Road Embankment Construction: Comparison of Lignin and Lime Soil Stabilization Treatments. Sustainability 2023;15:1912. https://doi.org/10.3390/su15031912.